C6-673/33 2

Volume I
Technical Summary Report

Study of Structural Bending Adaptive Control Techniques for Large Launch Vehicles

Contract No. NAS8-20056

Prepared for George C. Marshall
Space Flight Center

Huntsville, Alabama 35812

March 16, 1966

AUTONETICS
A DIVISION OF NORTH AMERICAN AVIATION, INC.

DATA SYSTEMS DIVISION
Department 345-4
P.O. Box 4171
3370 Miraloma Avenue
Anaheim, California 92803

FORM A 158

FOREWORD

This document is the Technical Summary Report for the Study of Structural Bending Adaptive Control Techniques for Large Launch Vehicles performed under NASA Contract NAS8-20056. A second volume provides all technical data in support of this report, including vehicle data and equations of motion.

The study program was sponsored by the NASA George C. Marshall Space Flight Center, Huntsville, Alabama and was performed by the Data Systems Division of Autonetics, a Division of North American Aviation, Inc. The cognizant NASA Project Engineers were Messrs. Jerry Redus and John Livingston of the Astrodynamics and Guidance Theory Division of the Aero-Astrodynamics Laboratory, George C. Marshall Space Flight Center, Huntsville, Alabama. This was a 14-month program beginning on January 19, 1965 and ending March 31, 1966.

At Autonetics, the program was performed by the Advanced Engineering Department of the Data System Division. Mr. J. M. Johnson, Jr. was the project leader and Messrs. R. K. Crow and C. L. Lutes were co-principal investigators. Acknowledgement is made of the valuable contributions provided by Miss J. Potter of the Data System Division.

TABLE OF CONTENTS

ILLUSTRATIONS

ILLUSTRATIONS (cont'd)

I. SUMMARY

This report presents the major results of the Study of Structural Bending Adaptive Control Techniques for Large Launch Vehicles performed under NASA Contract NAS8-20056. NASA Model Vehicle II data was used for the dynamic representation of the launch vehicle. A more complete description of the study and results can be found in Volume II. The system studied utilizes the principles of spectral identification to identify the vehicle dynamics and uses the identified parameters of the vehicle to compute the required control compensation for proper system performance and stability. Computations are performed digitally, and the functions of identification/compensation are performed continuously during vehicle operation. The study is devoted primarily to the problem of decoupling the elastic and the rigid body mode (passive control). However, a brief discussion on active bending control which is concerned with minimizing the actual vehicle bending through the use, in this case, of single force point control (main nozzles) is also included.

This report summarizes the overall study objectives, describes the basic spectral identification system and presents the significant study results. In addition, an Appendix section is included which shows the pertinent equations of motion.

The study results include the stability and trajectory analyses as well as the modifications to the basic spectral identification system which were necessary to satisfy the system requirements. The stability analyses results are presented in the form of gain-phase plots and were performed for three flight cases: lift off, maximum dynamic (q) pressure and end of first stage after launch. Satisfactory stability was achieved for all cases with the complete spectral identification system operative.

The trajectory results cover the complete first stage and show the dynamic behavior of the identification system and the ability of the vehicle to follow the trajectory in the presence of atmospheric disturbances and instrument noise. The trajectories are pitch plane digital simulations from lift off to the end of first stage with the digital compensation and frequency identification system functionally mechanized in the study as they would be in a digital control computer. The results indicate the capability of the system to provide stable control of a vehicle with wide margins of uncertainty in the vehicle dynamic and flexibility coefficients.

The study did not involve the details of the digital computer mechanization, however, preliminary estimates indicate that the complete spectral identification system requirements are well within the state-of-the-art of present day airborne digital computers. Memory capacity of approximately 2,000 words, word length of 16 bits and computational speed of 5u sec add time are some of the important requirements of the system.

I. SUMMARY (cont'd)

The overall features of the spectral identification adaptive control system are summarized as follows:

(1) the system identifies the desired bending mode frequencies with minimum a priori knowledge,
(2) the system is readily adaptable to control system requirements,
(3) the forward loop compensators are controlled continuously by means of the identified information,
(4) the system provides real time frequency information,
(5) the hardware problems associated with varying payloads and/or missions are minimized and,
(6) the system stability is assured

II. INTRODUCTION

The effective size of a boost vehicle designed for a space mission is measured by the usable payload pounds that can be placed in orbit. The major positive contributor to payload pounds is the weight and efficiency of the rocket propellant. The major negative contributor to payload pounds is the weight of the structure required to hold the propellant, engines and payload together. The best boost vehicle design thus minimizes the structural weight. Minimum structure results in increased vehicle flexibility (i.e., ability for the vehicle to bend). Increase flexibility has an adverse affect upon the performance of the attitude control system.

The purpose of the attitude control system is to measure the direction of vehicle travel and to maintain the direction desired by the guidance system in a manner that will not destroy the vehicle. A boost vehicle is similar to a long rod which bends in two ways when forces are placed upon it. The first is a steady state bend equivalent to the sag in a rod when it is supported horizontally at both ends. The second way is an oscillatory bend which would be exhibited by the rod if a weight were to be dropped on it while horizontally supported. This oscillatory bending tends to die out by itself unless it is being continually forced and excited. The control system in maintaining proper heading is continually applying forces to the vehicle. The control system must be designed so that in continually applying forces to the vehicle, it does not also continually excite the bending in a manner to increase bending deflections and ultimately destroy the vehicle. The attitude of the vehicle is measured by an instrument rigidly attached to the vehicle structure. The sensor measures not only the vehicle attitude but also the local vehicle bending at the sensor location. The attitude control forces computed from the sensor output are thus partially determined by the bending magnitude at the sensor. Factors depending upon the relative bending direction between the sensor locations and the attitude control force point, plus computational delays in computing the attitude control force magnitude from the sensor output determine whether the applied force increases or decreases any bending that may exist. The effects of computational delays are directly dependent upon the oscillatory frequency of the bending.

A normal control system for a flexible vehicle does not allow high frequencies to pass through to the force point, thus eliminating the reinforcing of high frequency oscillatory bending modes. Computational delays are so designed that the low frequency oscillatory bending modes are suppressed by the control forces rather than reinforced. However, with very large and very flexible vehicles, a normal control system design may be inadequate. For very flexible vehicles, the bending oscillatory frequencies become low enough that even the higher modes cannot be filtered out without detrimental effects upon the attitude control. With large vehicles, it is impossible to predetermine the bending oscillatory frequency to the accuracy required to adjust the computational delays in a manner to achieve guaranteed stable control.

A method of obtaining stable control under these adverse bending conditions would be to accurately measure the bending frequencies during flight and place notch filters in the control system at these frequencies so that just the bending frequencies are inhibited from contributing to the attitude control force. Even with perfect identification of the bending frequencies and with the notch filters tuned to these frequencies, the vehicle still bends as it is excited by forces other than the attitude control forces. Since this is the case, the sensor output in general contains signals representative of the oscillatory bending even with perfect control system notch filtering. If the power spectral density of the sensor output is measured, there would be peaks at the bending frequencies. It is the measurement of the frequencies of these peaks which are used during flight to tune the notch filters.

This report shows the results of applying this type system, Spectral Identification Adaptive Control System, to a realistic large launch vehicle in a complete closed loop trajectory simulation with bending frequencies changing and initial frequency uncertainties. The vehicle was subjected to realistic winds and gust inputs. Because of the large bulk of pertinent data generated during the study and the numerous minor details that were investigated, this summary report has been generated to briefly explain the system operation and present major study results. See Volume II for the complete final report.

III. STUDY OBJECTIVES AND GROUND RULES

The objectives of the study were to:

(1) Design a spectral identification system to achieve minimum coupling between bending modes and short period.
(2) Provide basic system stability.
(3) Achieve a practical mechanization of the final system.
(4) Demonstrate the Spectral Identification Adaptive Control System in a complete closed loop time varying trajectory simulation, including adaptive features working with vehicle bending frequency changes in combination with realistic wind and gust inputs.

The study ground rules were:

(1) The study was based on Model Vehicle II data received from George Marshall Space Flight Center, Huntsville, Alabama. Figure 1 is a pictorial representation of Model Vehicle II.
(2) The study was restricted to the pitch phase.
(3) The study was restricted to the first stage.
(4) The slosh dynamics are included in stability analyses.
(5) The dynamics of the system included short period mode, four flexible modes, engine compliance, sensors, actuator and fuel slosh.
(6) The bending frequencies were not restricted to a prescribed frequency band but a total bandwidth was defined which included all this bending modes of interest.

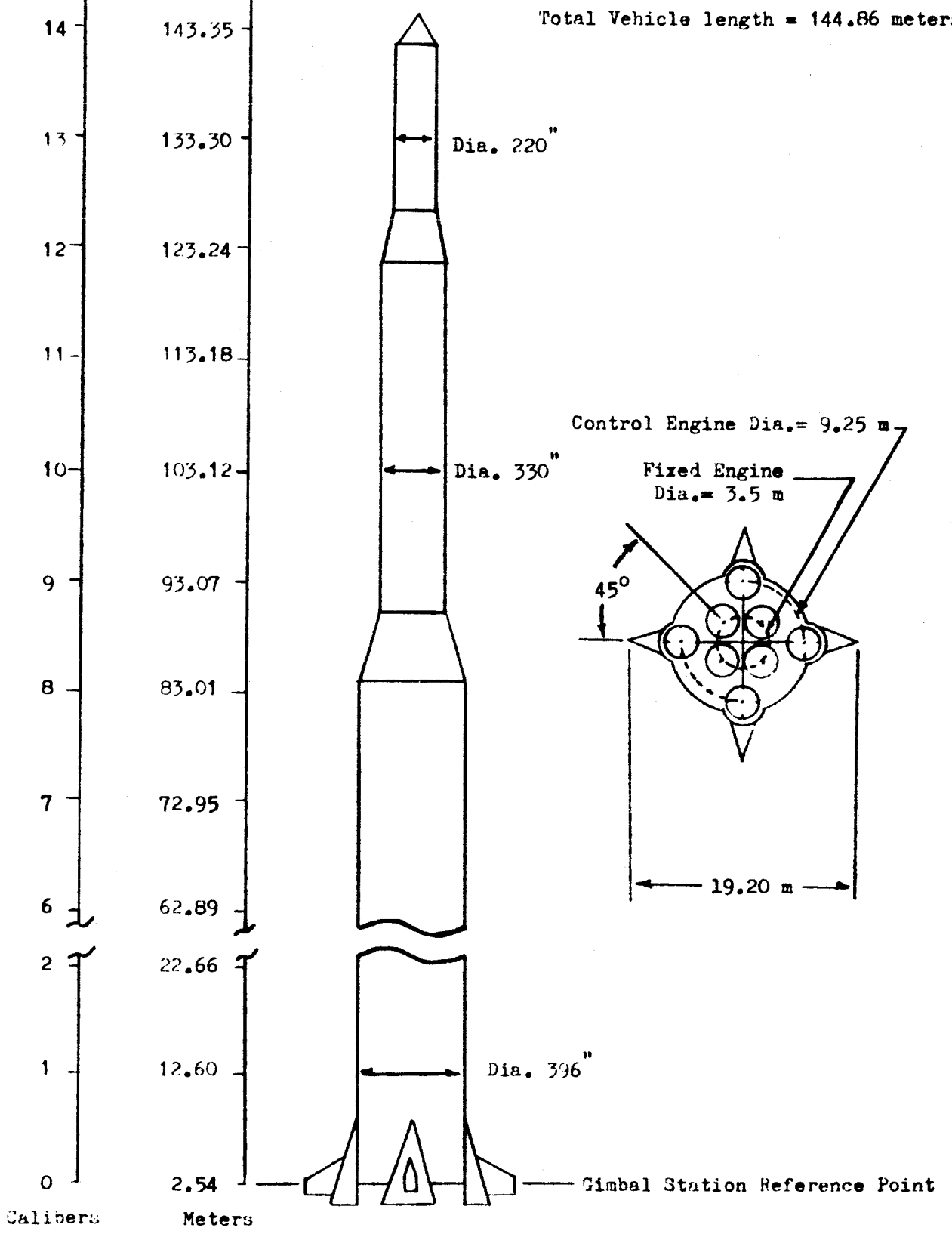

Figure 1. Model Vehicle No. 2

IV. SPECTRAL IDENTIFICATION ADAPTIVE CONTROL SYSTEM

The Spectral Identification Adaptive Control System includes a conventional short period control system where the attitude command is summed in the proper ratio with the output of an attitude gyro and attitude rate gyro. This composite error signal is filtered by a short period compensator and then filtered by three notch filters which eliminate the first, second and third bending mode components from the error signal. The output of the final notch filter is used as the deflection command to the main thrust nozzles. In order that the notch filters remove the bending, they must be tuned to the bending frequencies. The bending frequencies are initially unknown (but restricted to a band) due to uncertainties in the vehicle dynamics and change during the trajectory as propellant is expended. In order to insure that the notch filters are tuned to the bending frequencies, the bending frequencies are continuously identified during the flight. Figure 2 shows a block diagram of the spectral identification digital adaptive control system.

A. Frequency Identification System

The bending frequencies of the Model II vehicle are identified by placing 24 spectral filters tuned to 24 frequencies over the expected frequency band of the first three bending modes. The input to the filters is an instrument(s) (rate or acceleration) which contains signals at the bending mode frequencies in question.

Either an acceleration or a rate type instrument is acceptable for use with the spectral identification system. A single instrument may be used or two instruments may be used, one of which would be located near the front end of the vehicle and the other near the aft end. The single instrument configuration offers the potential of locating all the control/guidance sensors together while the two instrument configuration provides a better bending signal for the spectral filters since the rigid body information can be eliminated from the total signal.

The spectral filters, at or near the unknown bending frequency, have larger outputs than the other filters. Each spectral filter output for square wave kernels is the solution of equation (1).

$$A_i = \left[\sum_{j=1}^{\frac{2\pi N}{TW_i}} Ein\,(j \cdot T) \cdot sqs\,(W_i jT) \right]^2 + \left[\sum_{j=1}^{\frac{2\pi N}{TW_i}} Ein\,(j \cdot T) \cdot sqc\,(W_i jT) \right]^2 \qquad (1)$$

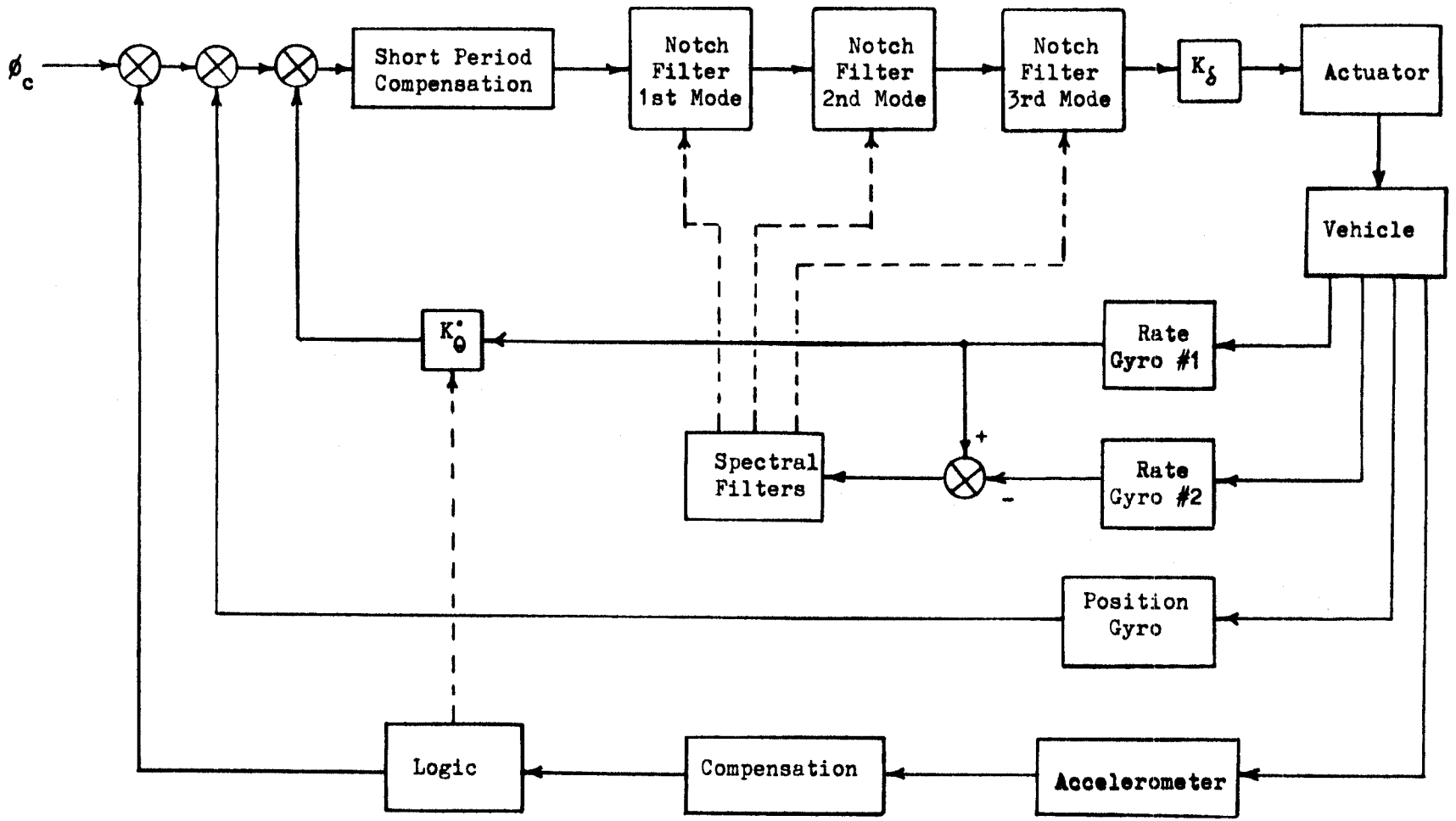

Figure 2. Spectral Identification Digital Adaptive Control System

where T is the sampling interval, N the spectral filter order and Wi the tuned frequency. The manner in which the summations are processed for the determination of the appropriate bending frequency is described later. Figure 3 is a block diagram of the spectral identification system.

Figure 4 shows the frequency identification performance for an ideal signal input of the form given by equation (2).

$$F(t) = B_1 \sin W_1 t + B_2 \sin W_2 t + B_3 \sin W_3 t \qquad (2)$$

where $B_1 = B_2 = B_3$ and the frequencies (W_1, W_2, W_3) change linearly with time as shown by the solid lines in Figure 4. The 24 spectral filters are tuned over the total frequency range from 1.51 rad/sec to 14.28 rad/sec, with a basic spectral sampling period of 0.01 sec. The filter outputs are initially used at order one and propagated to order 5. This choice of filter order is related to the initial speed of response, the initial uncertainty factor associated with the mode frequencies, dynamics of the vehicle and compensation configurations. It should be mentioned at this point that it is impossible to state a number such as an equivalent time constant as a measure of the speed of response of identification. The speed of response for a particular bending mode is dictated by the amount of bending activity, the bending frequency and the required bending frequency identification accuracy which in turn is related to the overall system stability and dynamic performance. Therefore, for the final system design, the factors of frequency identification, system stability and dynamic performance cannot be separated but must be treated on a completely integrated basis.

The parameters and elements associated with the frequency identification system include:

(1) the spectral filters (total filters a function of number of bending modes required to control and data uncertainty)
(2) the kernel function
(3) the variable integration period and sampling time
(4) the information processing center (method for determining identified frequencies)
(5) the smoothing filter (applied to output signal from processing center)
(6) the notch filter (tuned by identified information)

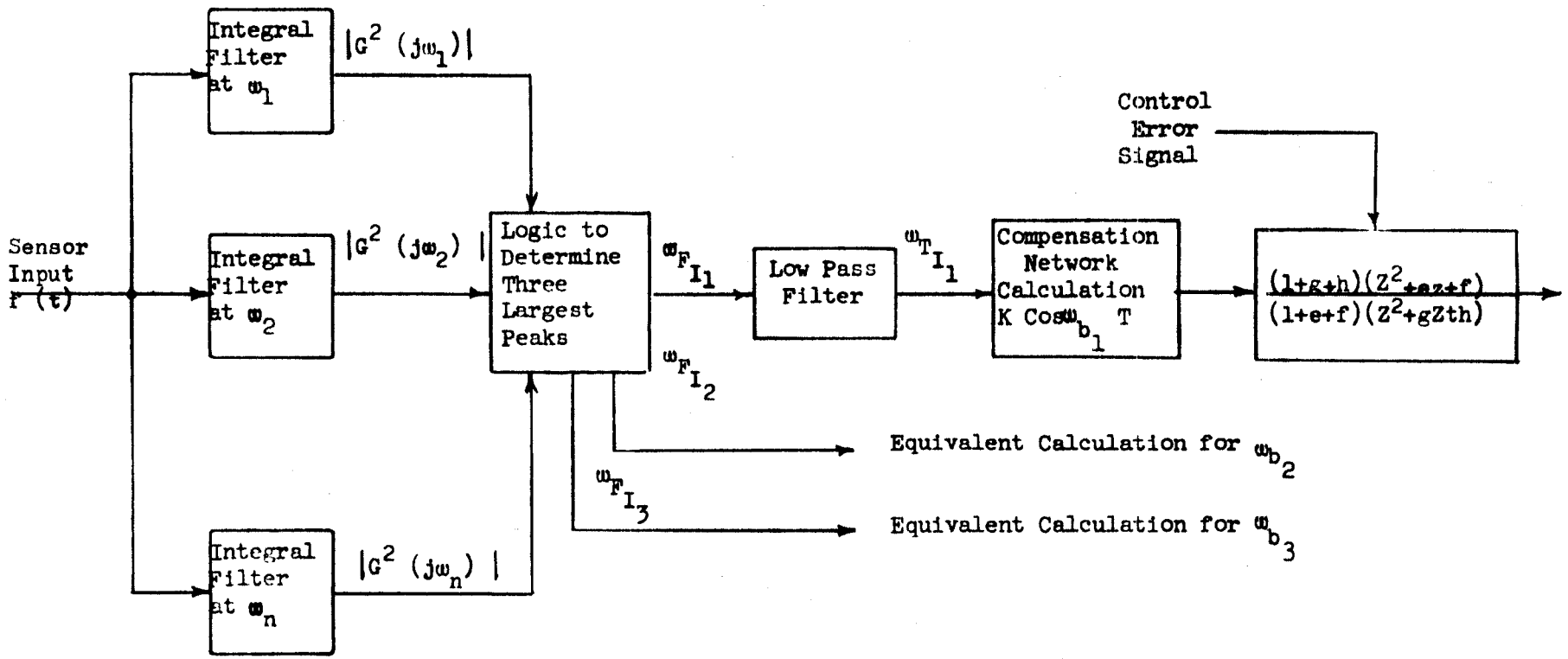

$$|G^2(j\omega_n)| = \frac{1}{T}\left(\left[\int_o^T P_1(\omega_n t) f(t)\, dt\right]^2 + \left[\int_o^T P_2(\omega_n t) f(t)\, dt\right]^2\right)$$

Figure 3. Spectral Filters and Frequency Identification System

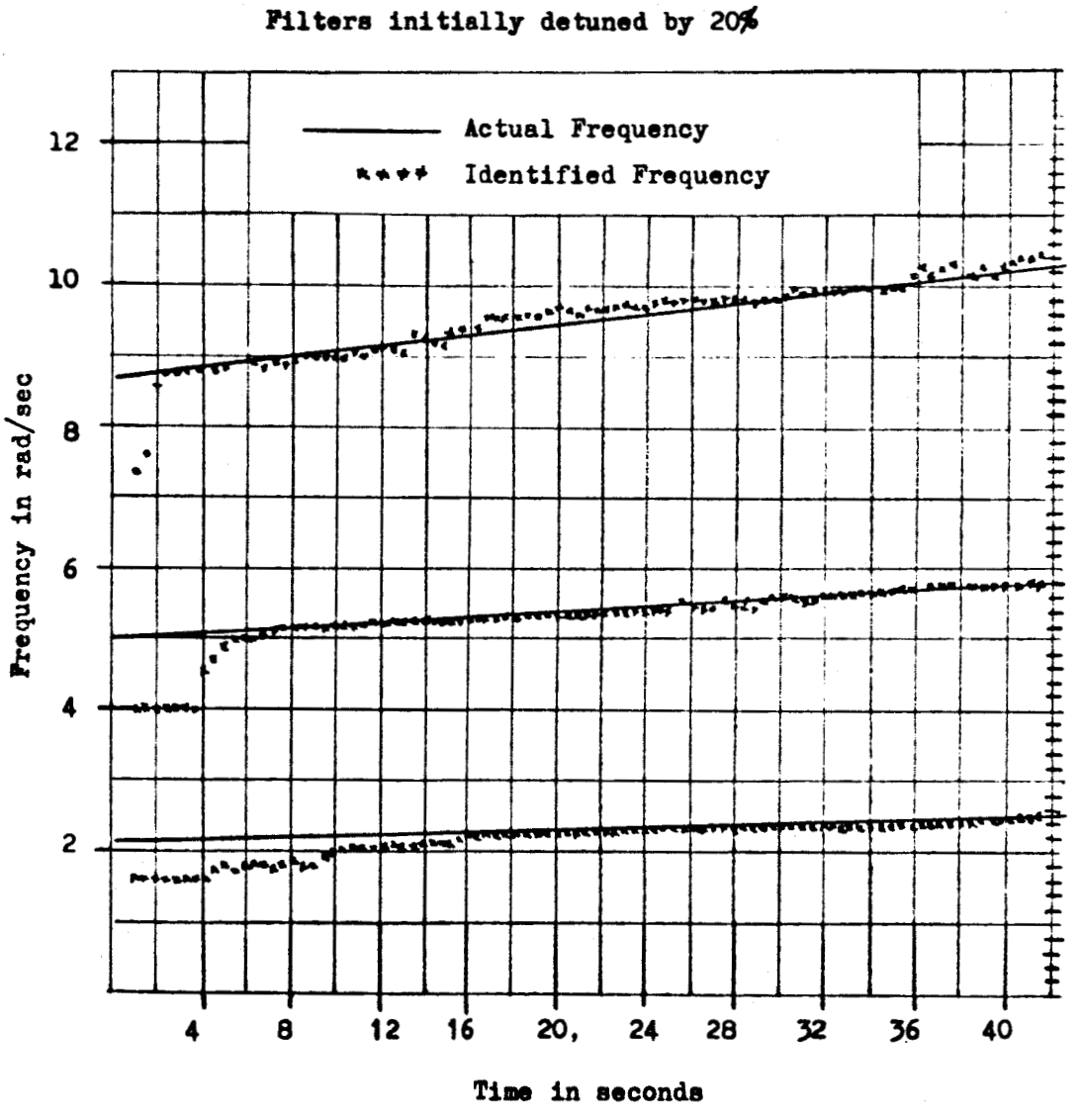

Figure 4. Spectral Identification System Performance - Ideal Signal Input

B. SPECTRAL FILTERS

The operation of each spectral filter can be explained by reference to Fourier Integral Theory.

A periodic function of time, f(t), of periodicity ℓ seconds can be written as a Fourier Series sum of sine and cosine functions[1] by equation 3.

$$f(t) = \sum_{n=0}^{\infty} A_n \sin\left(\frac{n\pi t}{\ell}\right) + \sum_{n=0}^{\infty} B_n \cos\left(\frac{n\pi t}{\ell}\right) \tag{3}$$

where

$$A_n = \frac{2}{\ell}\int_0^{\ell} f(t) \sin\left(\frac{n\pi t}{\ell}\right) dt \tag{4}$$

$$B_n = \frac{2}{\ell}\int_0^{\ell} f(t) \cos\left(\frac{n\pi t}{\ell}\right) dt \tag{5}$$

If the function f(t) is non-periodic then it cannot be represented by a summation of periodic frequencies but contains components at all frequencies. A_n and B_n are the sine and cosine discrete frequency amplitudes for the periodic case and become continuous functions of frequency, ω, for the non-periodic case. These functions are

$$A(\omega) = \frac{2}{\pi}\int_0^{\infty} \sin(\omega t) f(t)\, dt \tag{6}$$

$$B(\omega) = \frac{2}{\pi}\int_0^{\infty} \cos(\omega t) f(t)\, dt \tag{7}$$

The function f(t) can then be expressed as

$$f(t) = \int_0^{\infty} A(\omega) \sin(\omega t)\, d\omega + \int_0^{\infty} B(\omega) \cos(\omega t)\, d\omega \tag{8}$$

$A(\omega)$ and $B(\omega)$ thus represent the sine and cosine amplitudes of f(t) at the frequency ω and the total squared amplitude at the frequency is $A^2(\omega) + B^2(\omega)$.

The theory behind the generation of the spectral filter output is to determine an approximate squared amplitude at a frequency, ω_o, for a time slice of a sensor output. At time slice of the sensor output is used because the purpose of the spectral is their use in a system

1. Morse, Philip M., and Feshback, Herman: "Methods of Theoretical Physics," Volume 1, pp. 454-455, McGraw-Hill, New York, 1953.

to identify frequencies which change in time; therefore, a time slice is taken which is long enough to include several periods of ω_o but short enough so that the frequency to be determined does not change significantly. Figure 5 shows a typical differential rate gyro output and the time slice used to generate a spectral filter output for ω_o, where p is one-half period of ω_o. The dashed line represents the time slice of the input function which is defined as f(t). Thus f(t) has a value between t_o and 2pn + t_o and is zero everywhere else. Equations 6 and 7 then become

$$A(\omega) = \frac{2}{\pi} \int_{t_o}^{t_o+2pn} \sin(\omega t)\, f(t)\, dt \qquad (9)$$

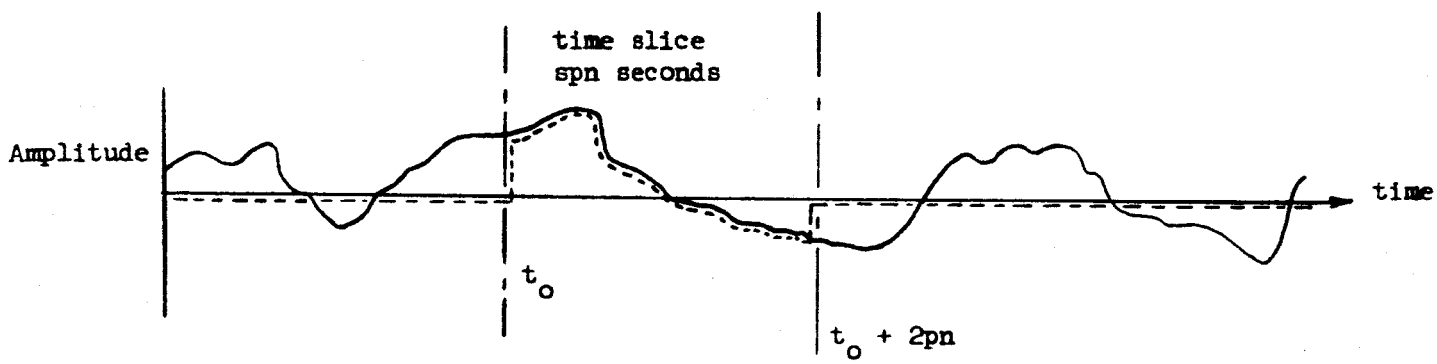

Figure 5. Typical Spectral Filter Input Time Slice

and

$$B(\omega) = \frac{2}{\pi} \int_{t_o}^{t_o+2pn} \cos(\omega t)\, f(t)\, dt \qquad (10)$$

Since the spectral filter evaluates A(ω) and B(ω) at only the frequency point ω_o, ω_o can be substituted into Equations 9 and 10.

C. KERNEL FUNCTIONS

Solutions for $A(\omega_o)$ and $B(\omega_o)$ are developed in a digital computer at a rapid sampling rate. The sin $(\omega_o t)$ and cos $(\omega_o t)$ kernel functions are costly to form in a digital computer if they are required at a fast rate. In evaluating the sin $(\omega_o t)$ and cos $(\omega_o t)$ either the series expansion for sine and cosine must be evaluated or a difference equation solution must be used to propagate the functions. The fastest way is to use a difference equation solution since ω_o and the sampling rate are fixed for each spectral filter. To do this requires four multiplications and two additions to propagate the sine-cosine pair a single increment in time. The sampling rate required for Model Vehicle II at which the sine-cosine propagation would have to be conducted is 0.01 seconds. The total number of* spectral filters used is 24. If a flight computer were used with computational speed capabilities equivalent to the IBM 7094, 0.002 seconds of computation time would be required to propagate the sine-cosine pairs for all 24 spectral filters. This amounts to 20 percent of the available computation time.

If, instead of using a sine and cosine function, a square wave kernel function of the same frequency is used, an approximation of Equations 9 and 10 is maintained at a significant reduction in computational complexity. A square wave can be propagated by testing for the time when it changes from +1 to -1 and -1 to +1. Thus, the 4 multiplications and 2 additions are eliminated from the requirements. In addition, if sine and cosine waves are used, they must be multiplied by f(t) before the integration is made. With square waves of amplitude ± 1 a multiplication is not required, but only a change in sign of the integration as the square wave changes sign. Thus, two kernel functions are defined

$$\text{sqs}\ (\omega t) = \frac{\sin \omega t}{|\sin \omega t|} \tag{11}$$

and

$$\text{sqc}\ (\omega t) = \frac{\cos \omega t}{|\cos \omega t|} \tag{12}$$

That is sqs (ωt) is a square wave in phase with sin (ωt) and sqc (ωt) a square wave in phase with cos (ωt). Using these kernel functions $A(\omega_o)$ and $B(\omega_o)$ become

$$A(\omega_o) = \frac{2}{\pi} \int_{t_o}^{t_o + 2pn} \text{sqs}\ (\omega_o t)\ f(t)\ dt \tag{13}$$

*Number of filters used were not optimized.

$$B(\omega_o) = \frac{2}{\pi} \int_{t_o}^{t_o+2pn} \text{sqc}\ (\omega_o t)\ f(t)\ dt \qquad (14)$$

The Fourier Series of sqs $(\omega_o t)$ is

$$\text{sqs}\ (\omega_o t) = \frac{2}{\pi} \left(\sin \omega_o t - \frac{1}{3} \sin 3\ \omega_o t + \frac{1}{5} \sin 5\ \omega_o t + \ldots\right) \qquad (15)$$

Comparing the values of $A(\omega_o)$ developed from Equation 13 and $A(\omega_o)$ developed by Equation 9 by substituting Equation 15 into Equation 13 we find

$$A(\omega_o)_{sqs} = \frac{2}{\pi} A(\omega_o)_{sin} - \frac{2}{\pi} \left(\frac{1}{3}\right) A(3\omega_o)_{sin} + \frac{2}{\pi} \left(\frac{1}{5}\right) A(5\omega_o)_{sin} \ldots \qquad (16)$$

Equation 16 shows that when square wave kernels are used the amplitude of the frequency component at ω_o is found but distorted by the amplitude components at $3\omega_o$, $5\omega_o$, $7\omega_o$, etc. These higher frequency components are down by a factor of $\frac{1}{3}$, $\frac{1}{5}$, $\frac{1}{7}$, etc. Another way of viewing this is that Equation 9 determines the magnitude of the sin $(\omega_o t)$ component in $f(t)$ while Equation 13 determines the magnitude of the sqs $(\omega_o t)$ component in $f(t)$.

In the application of the spectral filters the time slice is chosen so that t_o always occurs when the sqs $(\omega_o t)$ changes sign. The time slice was chosen to be 5 periods of the spectral filter tuned frequency. The spectral filter output was computed from the equation set:

$$S_i = - \int_{t_o}^{t_o+ip} (-1)^i\ E_{in}(t)\ dt \qquad (17)$$

$$C_i = - \int_{t_o}^{t_o+ip/2} (-1)^i\ E_{in}(t)\ dt + \int_{t_o+ip/2}^{t_o+ip} (-1)^i\ E_{in}(t)\ dt \qquad (18)$$

$$U_i = S_i + S_{i-1} \qquad (19)$$

$$V_i = C_i + C_{i-1} \qquad (20)$$

$$S = \frac{1}{p\ell} \sum_{i=1}^{\ell} U_i \qquad (21)$$

$$C = \frac{1}{p\ell} \sum_{i=1}^{\ell} V_i \qquad (22)$$

$$A = S^2 + C^2 \qquad (23)$$

Descriptively the solution of these equations is: S_i is the integral over 1/2 period (p) of a square wave kernel times the spectral input signal with the kernel phased to change sign at t_o. C_o is the integral of the square wave kernel times the spectral input signal with the kernel phased to change sign at $t_o + p/2$. The kernel used in determining C_1 is in quadrature with the kernel used in determining S_i. U_i being the sum of S_i and S_{i-1} is thus the integral of the kernel times the spectral input signal with the integration period a complete period of the spectral filter tuned frequency. A value of U_i is computed for each half period time point, however. V_1 is equivalent to U_i except computed using the quadrature kernel. S is the sum of ℓ past values of U_i times a normalizing constant which removes the normal decrease in an integrator output with increase in input frequency. C is equivalent to S except computations are made using V_i instead of U_i. The total spectral filter output is then computed by taking the sum of the squares of S and C.

D. Spectral Filter Frequency Response

Figure 6 is the output amplitude of a spectral filter as the input frequency is varied. The amplitude is plotted versus normalized frequency, r, computed by dividing the input frequency by the tuned frequency. The spectral filter response is dependent upon the phase relationship between the input frequency and the square wave. Figure 6 shows two curves, one drawn with a continuous line and the other with a dashed line. These two curves represent the extremes in spectral filter gain as the input signal phase changes. The integration period was 5 periods (i.e., $\ell = 9$).

E. Spectral Filter Information Processing

Since there are 24 spectral filters, there are 24 values of A computed which are distinguished from each other by the subscript n (i.e., A_n) corresponding to the spectral filter tuned frequencies (ω_n) and the number of samples m_n in the 1/2 period using a 0.01 sec sampling time shown in Table 1. Because the spectral filter output amplitudes should be greatest when the spectral filter tuned frequency is near a

Figure 6. Spectral Filter Frequency Response

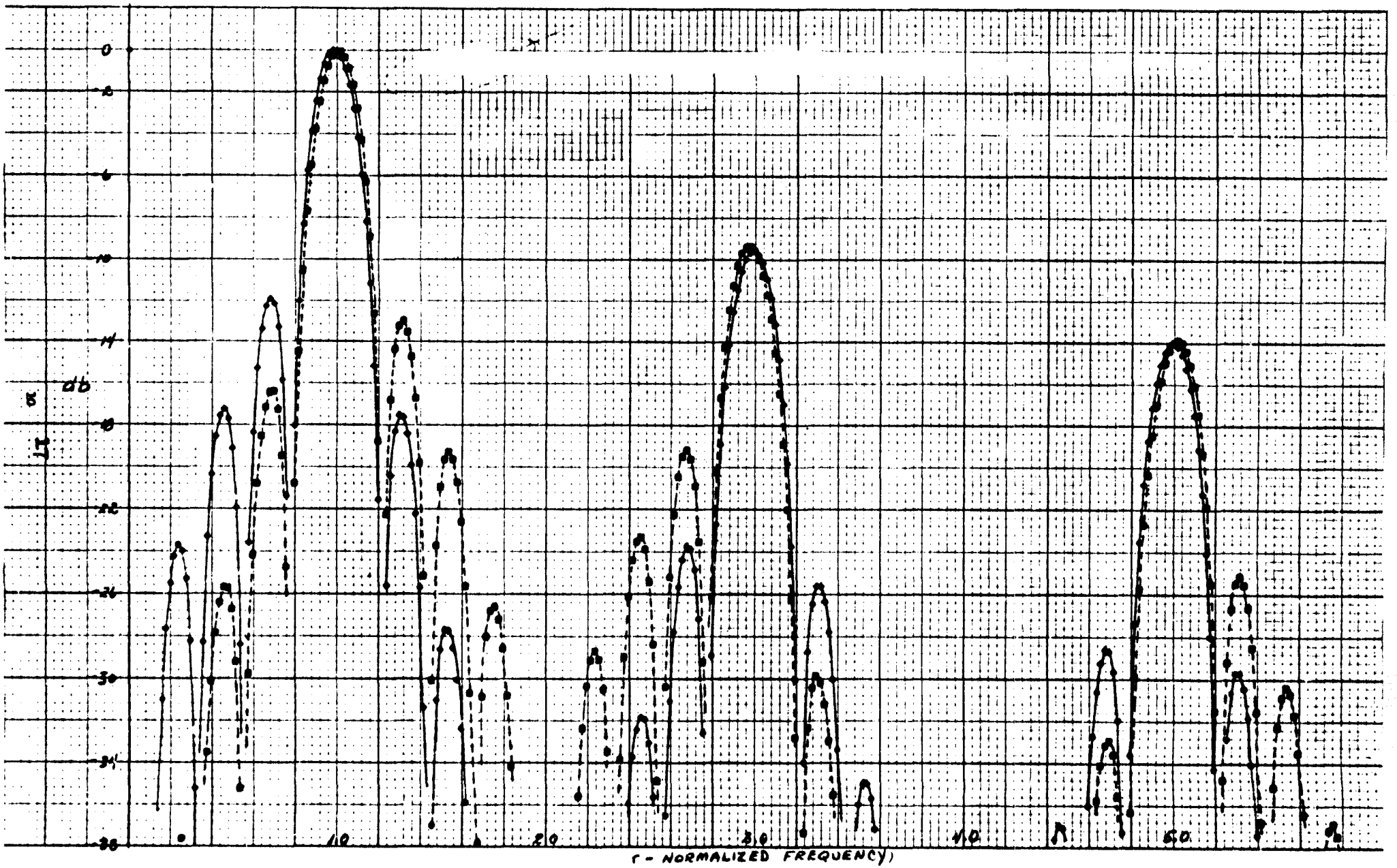

bending frequency amplitude, peaks in the A_n array are used to determine the bending frequencies. The following step by step procedure is used in determining the bending frequencies.

1. All values of A_n smaller than a set of resolution values are set equal to zero. This is done to eliminate the identification of any peaks if the total bending activity is very low. Under the conditions when bending activity is low and resolution levels not present, frequency identification would be based mostly upon system noise. This could cause the notch filters to become detuned enough to produce unstable bending. The bending activity would immediately pick up and proper identification is made before the vehicle loads are exceeded; however, the total bending activity is greater than when the resolution levels are set.

n	m_n	n rad/sec
1	22	14.28
2	24	13.09
3	26	12.083
4	28	11.22
5	30	10.472
6	32	9.81
7	36	8.73
8	40	7.85
9	44	7.14
10	48	6.54
11	54	5.82
12	60	5.24
13	66	4.76
14	74	4.25
15	82	3.83
16	92	3.41
17	100	3.14
18	112	2.8
19	124	2.53
20	138	2.28
21	154	2.04
22	170	1.85
23	188	1.67
24	208	1.51

Table I. Spectral Filter Tuned Frequencies

2. The three largest peaks are determined from the complete A_n array. A value of A_n is a peak only if $A_n > A_{n-1}$ and $A_n > A_{n-2}$ and $A_n > A_{n+1}$ and $A_n > A_{n+2}$, i.e., A_n is a peak only if it is larger than two values of A on each side of A_n. In general, the amplitude of the peak associated with the first bending mode is larger than the peak associated with the second mode which is in turn larger than the peak associated with the third mode. It is not uncommon to have several spectral filter amplitudes in the vicinity of the first mode frequency be larger than any other of the spectral filter amplitudes. If A_n were to be compared with only a single spectral filter output on each side of itself, there would be at times a situation where A_{n+1} was less than A_n and A_{n+2} in the neighborhood of the first bending mode. In this case, A_{n+2} would be identified as a peak along with A_n and the peak at A_{n+2} would be larger than either the second or third bending mode peaks. The frequencies associated with A_n and A_{n+2} would both be identified and thus two notch filters would be placed in the vicinity of the first bending mode. This condition is eliminated when two values of A on each side of the peak value are required to determine a bending mode. For this case, the two filters on each end of the array (i.e., A_1, A_2 and A_{23}, A_{24}) constitute a special case. Filters A_1 and A_{24} are never candidates for a peak while a peak at A_2 exists if $A_2 > A_1$ and $A_2 > A_3$ and $A_2 > A_4$ and a peak exists at A_{23} if $A_{23} > A_{24}$ and $A_{23} > A_{22}$ and $A_{23} > A_{21}$. If more than three peaks are identified, only the three largest peaks are considered legitimate. With three peaks identified, the peaks are arranged in ascending orders of n and tentatively associated with the third, second and first bending modes, respectively.

3. If less than three peaks are identified, special processing must be performed to determine which bending mode peaks are associated with a particular bending mode. The last values of n determined for each mode are compared with the present values of n. The present identified peaks are then associated with the bending mode whose past value is nearest the present value of n.

4. At this time, 0, 1 and 2 or 3 peaks have been identified and tentatively, in each case, associated with a bending mode. A further test is made to determine if the identification is acceptable. It is known that for a real vehicle, except at the time of staging, the bending frequencies change in a more or less continuous manner. For this reason, the present identified n value for each bending mode is compared with the previous n value associated with that filter. If the difference between the present and past n values is greater than 7, the presently identified peak is rejected as being unacceptable.

5. If the change between the present value of n and the past value of n is between 4 and 7, it is limited to a change of no more than 3.

6. The vehicle bending mode frequencies are more or less harmonically related to each other within a tolerance band. This relationship is used to keep the mode identifications separated within the tolerance band. The ratio of ω_n at the second bending mode to ω_n at the first bending mode is compared with a fixed constant such that if the ratio is less than the constant, the second mode identification is rejected. A second test is made between the first and third mode with the third mode identification being rejected when the test fails.

7. At this time, a frequency is computed for each identified mode from the formula

$$\omega_{F_I} = \frac{A_{n-1}\ \omega_{n-1} + A_n\ \omega_n + A_{n+1}\ \omega_{n+1}}{A_{n-1} + A_n + A_{n+1}} \qquad (24)$$

8. ω_{F_I} for each mode is filtered to remove high frequency noise on the identified frequency by the formula

$$\omega_{T_{I_n}} = .5\ \omega_{F_{I_n}} + .5\ \omega_{T_{I_{n-1}}} \qquad (25)$$

ω_{T_I} is then used as the frequency to tune the notch filers.

The complete process is a rather complicated procedure though much has been done to reduce the computer speed requirements. At a .01 second sampling rate the integrations of Equations 17 and 18 are performed using a rectangular integration algorithm. Also at .01 second, testing is made to determine if the time to +ip/2 or t_o + ip has arrived (i.e., the upper integration limits).

This is the only computation for each spectral filter that is done at the .01 sampling rate if the upper integration time has not arrived. When the upper limit integration time t_o + ip/2 on the first integral in Equation 18 arrives, a change in sign of the kernel is made. When the upper limit integration time t_o + ip arrives for any spectral filter, the computations of U_i and V_i are made and S_i and C_i for the spectral filter reset to zero. At a sampling rate of .411 seconds the remainder of the computations and testing to determine ω_{T_I} are made.

Special considerations are required when the identifiers are started at launch. All past values of U_1, V_1, S_i and C_i are set equal to zero. The ω_T frequencies are initialized to the expected launch bending frequencies. A time long enough so that the first 10 spectral filters can compute their first values of C_1 and S_i (.48 seconds) must elapse before any identification of a new frequency is attempted and then only the third mode frequency. A time long enough for the first 15 spectral filters to obtain a complete C_i and S_i computation (.82 seconds) elapses before the third and second bending modes are allowed to be identified and total of 2.08 seconds elapses before all three modes are identified. Since the initial summations of U_i and V_i do not contain a total of 9 (the value of used in the system) terms, the normalizing constant for computing S and C is adjusted for each spectral filter.

F. Notch Filter

Upon identifying and smoothing, W_{T_I} the identified frequency for each mode is used to adjust the frequency sensitive coefficient in each of three forward loop notch filter networks. The Z transform representation of a forward loop notch filter is shown in equation 26.

$$D(Z) = K \frac{Z^2 - 2rZ\cos\omega_T T + r^2}{Z^2 + aZ + b} \qquad (26)$$

Where ω_T is the filter tuned frequency, K is the adjustable gain to give unity dc gain, T is the sampling period and r is the radius of the complex zero location in the Z plane which determines the sharpness and depth of the notch.

Figure 7 shows the amplitude versus frequency response of the notch filters used for each of the first three bending modes for the maximum dynamic pressure flight case (78 seconds after launch). The first bending mode filter is tuned to 2.3 rad/sec with r = .995. The second bending mode filter is turned to 5.6 rad/sec with r = .983 and lastly the third bending mode filter is tuned to 9.1 rad/sec with r = .975. The sampling frequency is 62.8 rad/sec, i.e. T = 0.1 sec. Associated with each filter mechanization are a pair of Z plane poles that are located within the unit Z plane circle by varying a and b as a function of the system stability requirements.

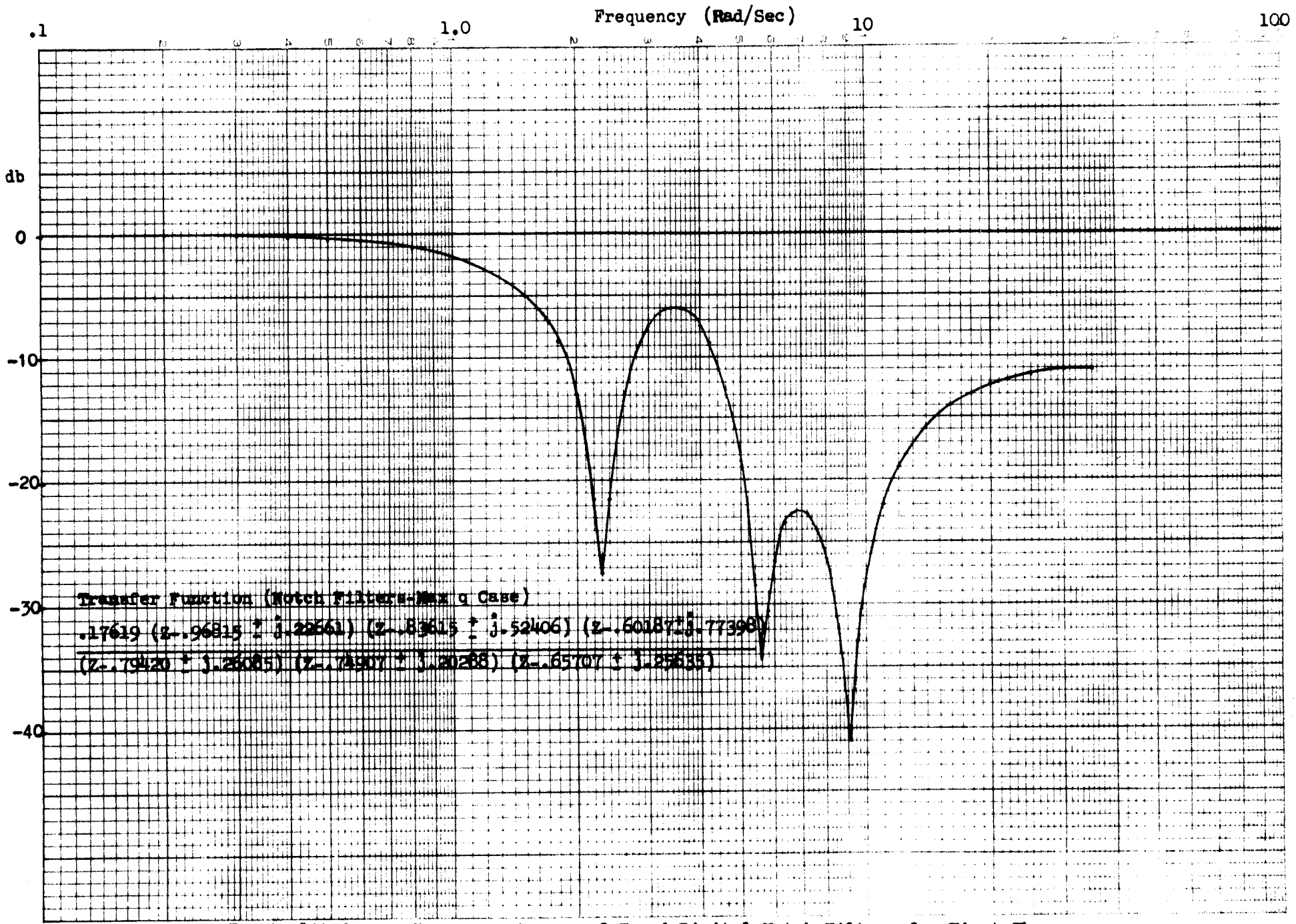

Figure 7. Amplitude vs. Frequency Curves of Tuned Digital Notch Filters for First Three Bending Modes - Maximum Dynamic Pressure Flight Case

V. CONTROL SYSTEM STABILITY ANALYSIS

The aim of the stability analysis is to determine a system compensation which maintains dynamic stability over the trajectory within the parameter uncertainties and the accuracy and speed of response properties of the frequency identification system.

The form of the compensation which evolved during the study consisted of a complex pole/zero compensator for each bending mode and a first order pole/zero for short period, all in the forward control loop. The adaptive loop adjusts the complex zero frequencies as a function of the identified bending mode frequencies.

A. System Compensation

The basic vehicle pitch control system is shown in Figure 8. The system feedback is composed of attitude position and attitude rate. This signal is fed through a short period compensator and 3 notch filters tuned to the first, second and third bending mode frequencies. Several basic control system designs were performed as the study progressed. These designs followed each other in a natural progression as additional insight into the total system was obtained with each individual control system studied. The results of the more optimum of these designs is presented in the following paragraphs of this summary report.

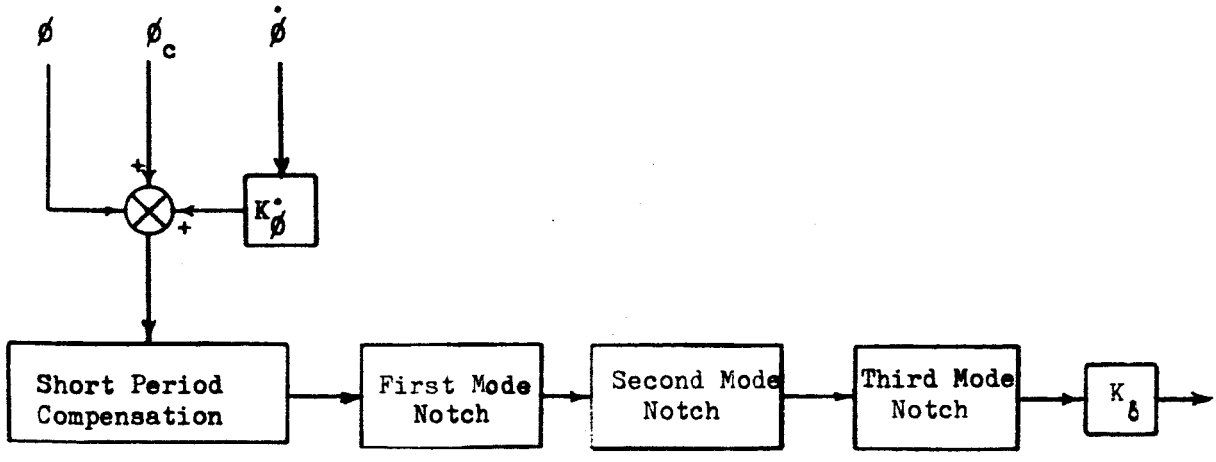

Figure 8. Basic Vehicle Control System

The problem of designing an optimum compensation configuration for compatibility with the frequency identification adaptive loop and the uncertainty factors associated with the vehicle data requires a series of tradeoffs which depend directly or indirectly on the following system considerations:

(1) The level of uncertainty associated with the vehicle data, especially bending mode frequencies, mode slopes and mode shapes.
(2) The typical variation of all of the vehicle parameters with trajectory time.
(3) The required trajectory following capability, i.e., the required short period control frequency.
(4) The vehicle structural load considerations.
(5) The speed and accuracy of the frequency identification system.
(6) The digital computer speed and resolution requirements for system mechanization.

Table II presents the control system constants. Figures 9, 10 and 11 are the open loop gain-phase plots for the three flight cases occurring at lift-off, maximum q and end of first stage using these control constants. In each case, the notch filters are tuned to the open loop bending frequency.

With perfect identification, the notch filters would tune to the closed loop bending frequency. Stability analyses of these three flight cases show that stability is maintained for $\pm$ 5% errors in bending frequency identification of all bending modes except the first bending mode at the end of first stage flight case (157 sec) where a + 3%, -5% identification error must be maintained.

Table II. Control System Constants

Sampling Rate	.1 sec
Rate gain	2.0 sec
Short period compensation	
Zero frequency	.4 rad/sec
Pole frequency	2.8 rad/sec

Notch filter parameters

Bending Modes		Damping	Frequency
1st Mode	Zero	.025	$\omega_{T_1}^*$
	Pole	.5	3.625 rad/sec
2nd Mode	Zero	.025	$\omega_{T_2}^*$
	Pole	.7	3.625 rad/sec
3rd Mode	Zero	.025	$\omega_{T_3}^*$
	Pole	.7	5.0 rad/sec

Loop gain: 0 to 112 sec 2.
112 to 144 sec 1.25
144 to 157 sec .61

* Identified frequency

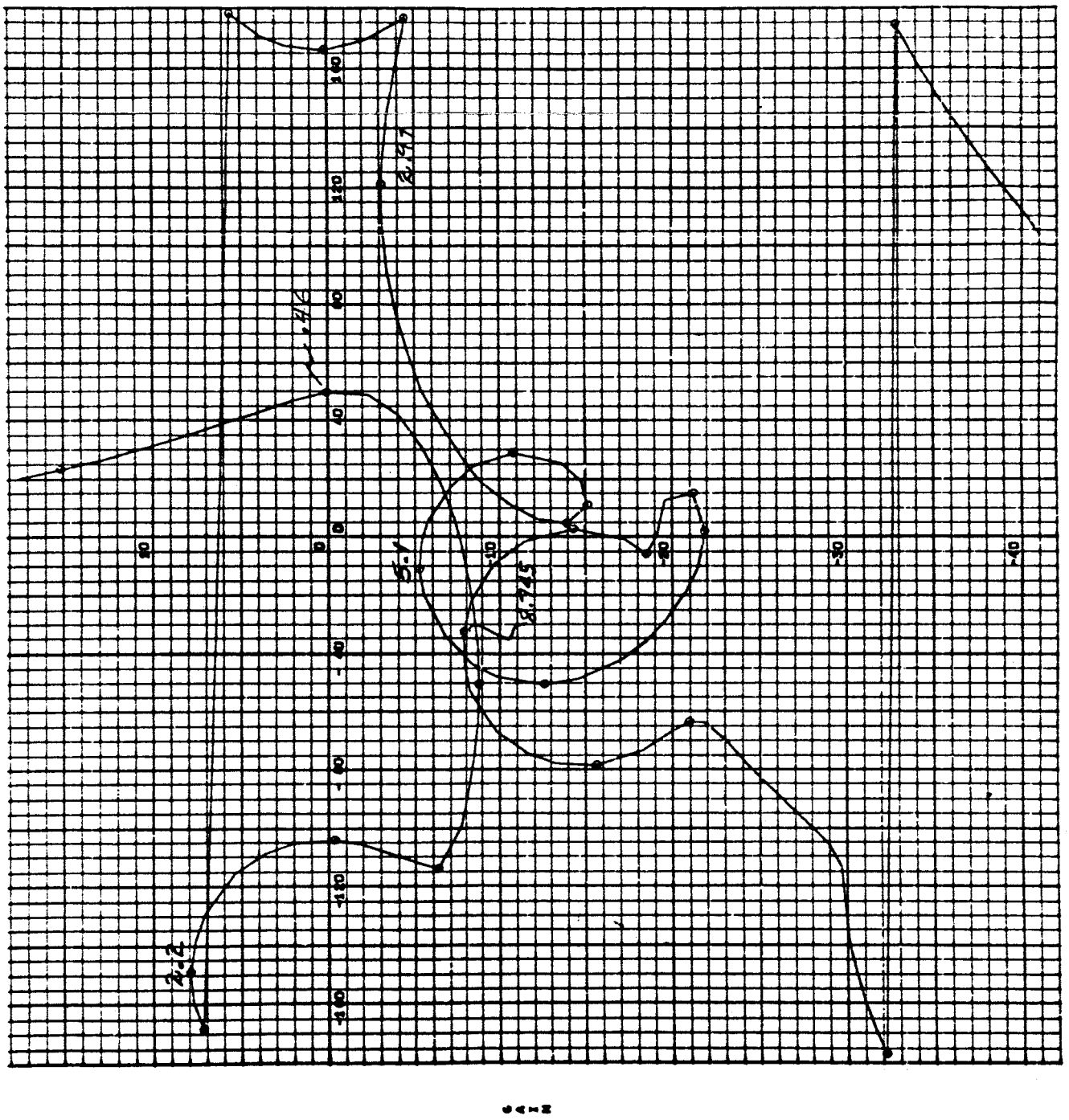

Figure 9. Open Loop Gain-Phase Plot For Lift-Off Flight Case With Bending/Short Period Compensation ($t = 8$ sec.)

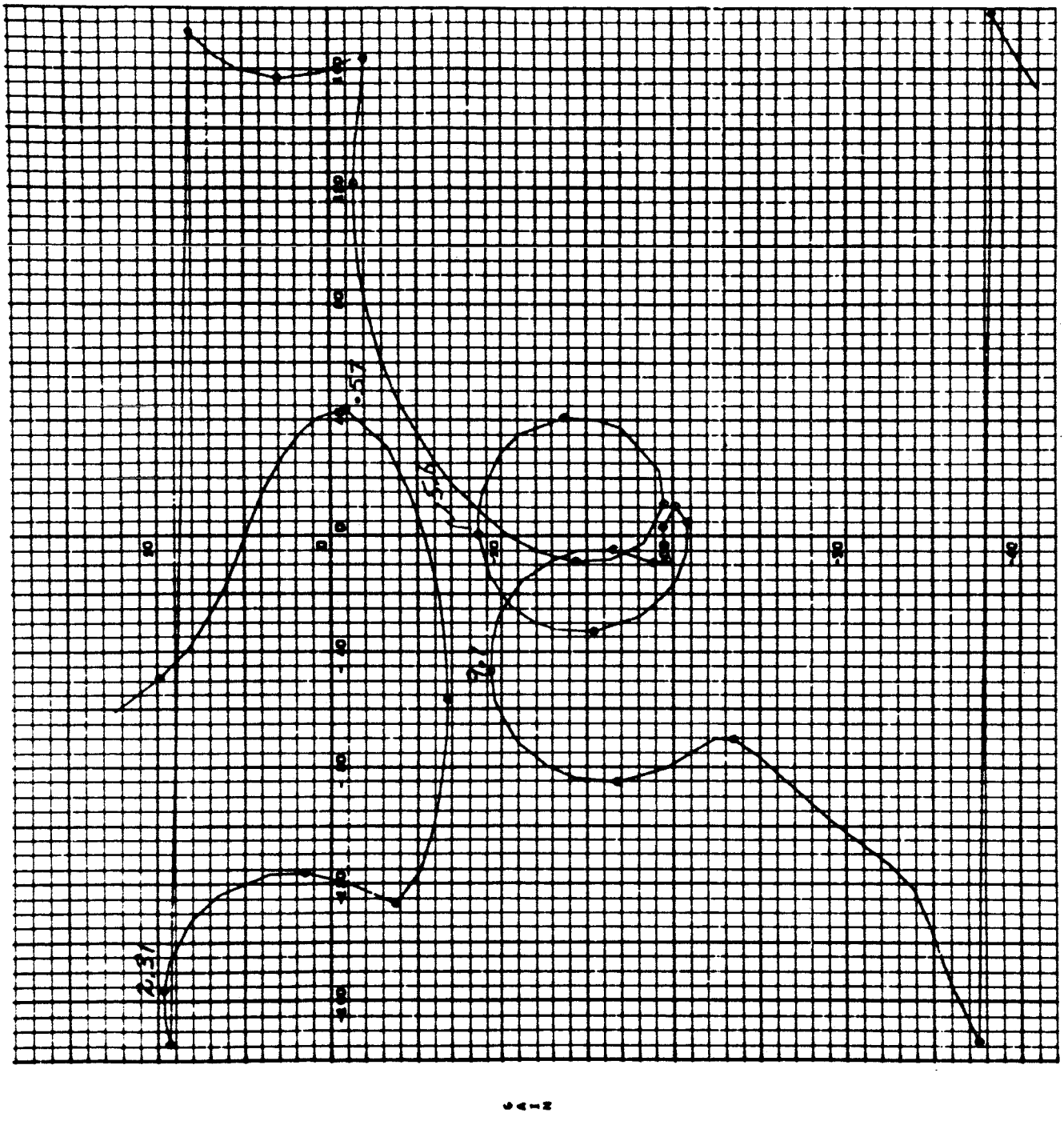

Figure 10. Open Loop Gain-Phase Plot For Max q Flight Case - With Bending/Short Period Compensation (t = 78 sec.)

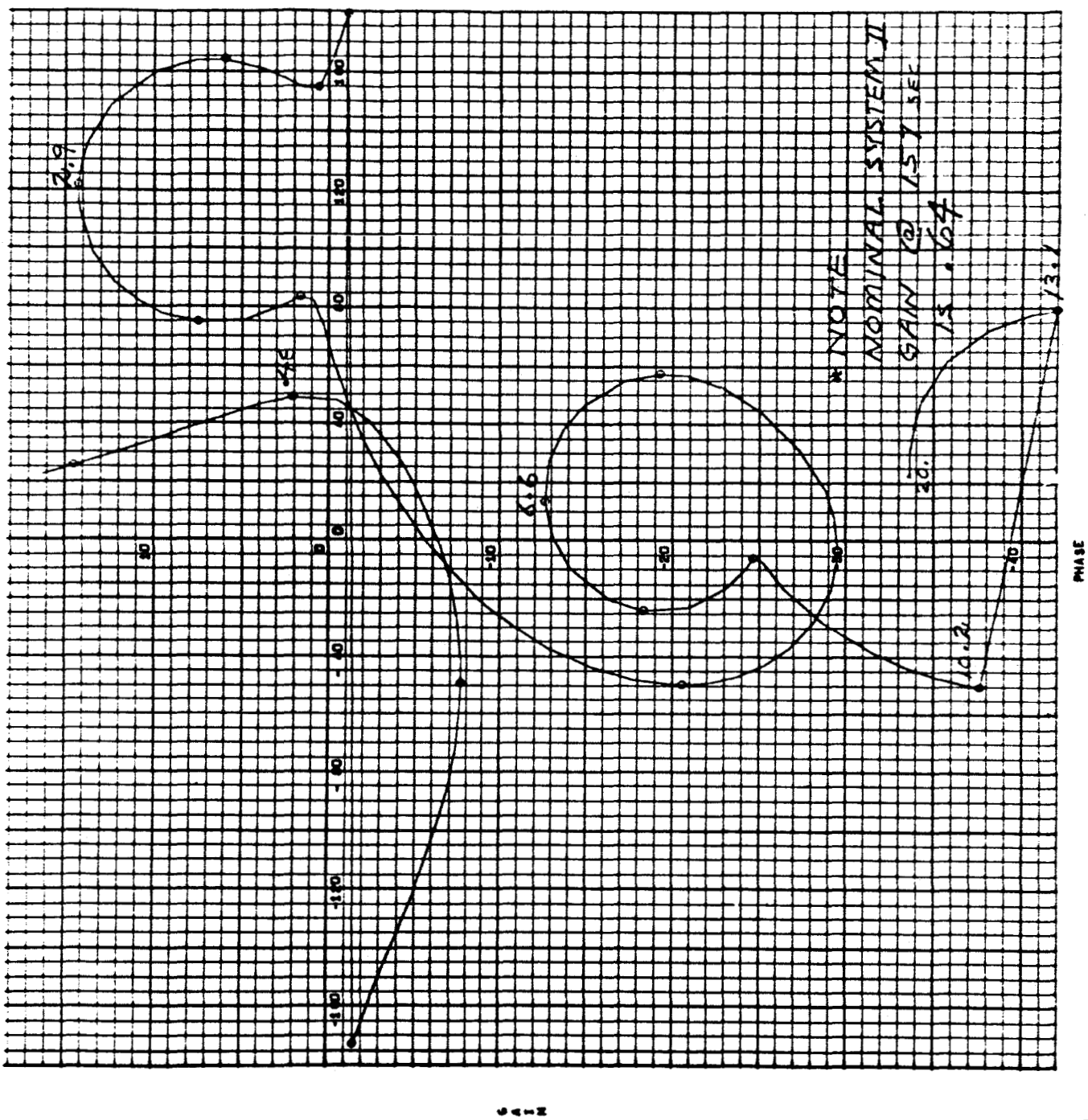

Figure 11. Open Loop Gain-Phase Plot For End Of First Stage Flight Case - With Bending/Short Period Compensation (t = 157 sec.)

An important question must be answered in determining the absolute stability of the control system in conjunction with the frequency identification system. If the identification system is operating perfectly, it identifies the closed loop bending frequency and moves the notch zero to this frequency. In moving the notch zero to the identified frequency, the control system is changed which in turn changes the closed loop bending frequency. At some place a null point exists where the notch zero frequency and the closed loop bending frequency are identical. The stability question that arises is the following: "Is the system stable when operating at this null point?" If the answer to this question is no, the control system is unacceptable. The control system specified by the parameters in Table II was investigated as to its stability with respect to this question and found to be stable. Some of the other control systems studied proved to be stable until this question was asked and then were proven to be unstable.

B. Slosh Effects

The stability plots shown in Figures 9, 10 and 11 include only three bending modes and no slosh modes. However, during the study a thorough stability analysis was made including a fourth bending mode and three slosh modes. It was determined that the fourth bending mode had little effect upon system stability and the slosh modes even with damping provided by baffled tanks, had a definite effect upon the system stability. The slosh effects reduced the bending mode phase margins and increased the bending amplitude peaks at some flight cases. With baffled tanks, the slosh did not produce an unstable system and simulation runs showed no adverse effects on the identification accuracy.

C. Worst Case Bending Parameter Analysis

A worst case bending parameter analysis was made where overall vehicle stiffness was varied by $\pm$ 10% and interstage stiffness by $\pm$ 50%. The effect of these variations on bending mass, frequency, slope and deflections were considered. In all cases, the short period and first bending mode remained stable. In only one case where the interstage stiffness was decreased by 50% and the overall stiffness increased by 10% did the second and third mode become unstable. This condition could easily be corrected by the introduction of 40° lag phase shift at the second bending mode and 5° lag phase shift at the third mode. This correction would introduce insignificant effects upon the short period and first bending mode stability.

D. Load Relief

The main purpose of the load relief system analysis was to demonstrate compatible operation with the spectral identification system. The principal features of the designed load relief system are:

(1) The system features a conventional normal acceleration loop, including second order digital compensation in the N_z loop.

(2) The load relief system becomes operative when the normal acceleration at the output of the N_z loop filter exceeds a threshold level.

(3) When the N_z loop is operative, the ordinary short period and bending compensation is unchanged but the N_z loop (in the control computer) includes the option of using a different rate gain and a (constant factor) gain adjustment on the system programmed forward loop gain.

Figure 12 is a gain-phase plot with the N_z loop closed for the maximum q flight case. The N_z compensation is second order, and includes (frequency characteristics) a pole at .3 rad/sec, a zero at 1 rad/sec and a second pole at 3 rad/sec. Equation 27 is the Z form of the N_z compensator.

$$DN_z\ (Z) = \frac{(Z-.90469)\ (Z+1)}{(Z-.97044)\ (Z-.73742)}\ \text{gain normalized} \qquad (27)$$

The N_z loop gain (actual) is +.368, the rate gain and system loop gain are respectively 3 and 1.1 when the N_z loop is operative. The N_z loop threshold used for the trajectory runs is 0.1 m/sec^2, monitored at the output of the dc gain normalized N_z loop filter. In the flight computer the N_z signal from the accelerometer (mounted at 46.54 m) is processed through the N_z filter from lift-off, and the output of the filter is tested at each control cycle time. When this signal exceeds the threshold specified, a different control equation, including the N_z term, the new rate gain and the N_z loop gain adjust are all processed by the control computer. When the N_z signal from the N_z filter goes below the threshold, the normal system control equation is again processed. This system results in a 37.7% reduction in peak loads due to wind disturbance. Additional load relief can be accomplished by increasing the short period frequency of the basic attitude control system. This increase in short period frequency of the attitude control loop would allow for higher load relief system gains and bandwidth.

The primary objective of establishing the adaptive system performance with load relief was achieved during this portion of the study.

E. Active Bending Control

Included in the study was an investigation of an active bending control system which utilized a differential rate gyro signal in combination with a desired compensation function which was derived on the basis of removing all bending excitation from the nozzle command signal without disturbing the short period response. This portion of the study was not completed in sufficient detail from which definite conclusions could be drawn. However, it was shown that for the one flight case analyzed, it was possible using single force point control, to achieve an equivalent rigid body/control system combination. However, the results were highly dependent upon vehicle parameter variations therefore, the utility of the method would depend on whether a fixed function could be generated to handle wide parameter changes and uncertainties or whether it would be necessary

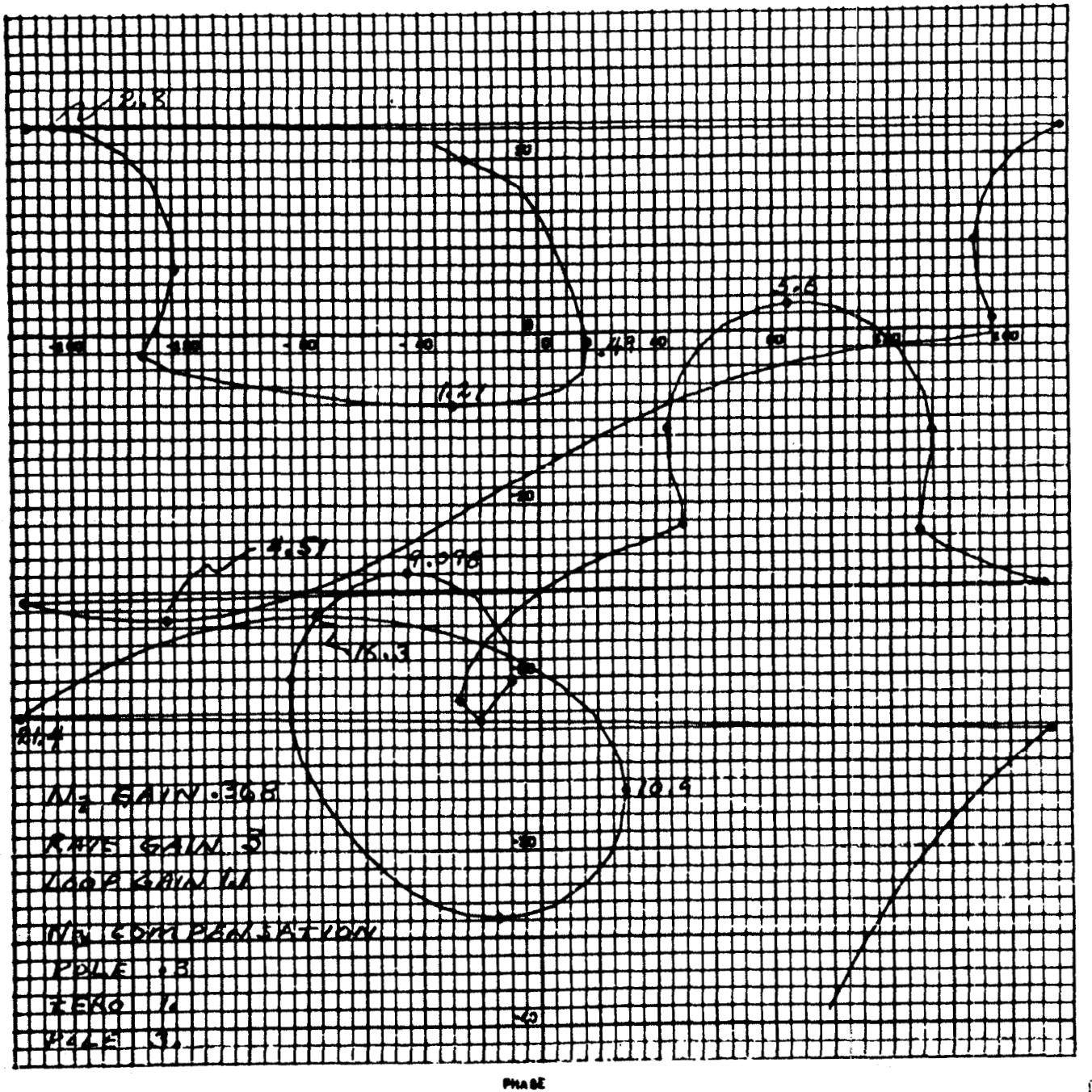

Figure 12. Gain-Phase Plot For Max q Flight case with bending/short period compensation - N_z loop closed

to continuously adapt the function to the changing environmental and off-nominal conditions. Figure 13 shows the basic idea of the active control system in open loop form. The differential rate gyro output is processed through the G(Z) compensation function and summed with the normal attitude control error signal to form the total nozzle command signal. The key to this system, as previously mentioned, is the method required to generate the appropriate compensation function throughout the flight regime.

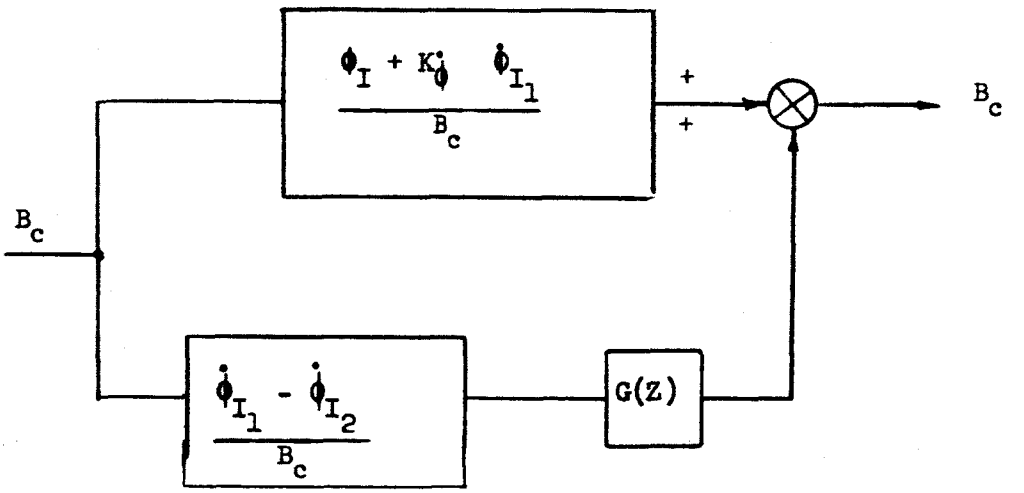

Figure 13. Open Loop Active Control System Block Diagram

VI. TRAJECTORY SIMULATION

A complete trajectory, i.e., t = 10 to t - 157 sec is shown in Figures 14 through 21. Trajectories were always started at t = 10 seconds rather than t = 0 seconds because with a digital simulation and the method used to mechanize the winds, there were no disturbances to the problem until pitchover occurred. The trajectory presented in Figures 14 through 21 initially has the notch filters tuned 25% low to simulate an initial uncertainty of the actual bending frequencies. At 52 seconds worst case MSFC winds are initiated with severe random wind gusts. Figure 22 shows the worst case MSFC wind profile. Initially with the notch filters tuned 25% low the first and third bending modes are unstable. The input signal to the spectral filters shown in Figure 18 is a measurement of bending only. This parameter shows that even though the first and third bending modes are initially unstable the initial speed of identification is rapid enough to obtain a stable configuration before the bending builds up to an unacceptable level. The initial instability was confirmed by stability analysis and trajectory runs where the notch filters were held fixed. Figure 14 shows the three identified frequencies and the open loop bending frequencies. The first bending mode is identified within 5% by t = 16 sec (i.e., 6 sec after the start of the run) and remains within this accuracy except during the high wind transient portion of flight and at the very end of the first stage flight where the open loop bending frequencies change rapidly. Since the second bending mode is of higher frequency, it should be more rapidly identified than the first mode. Figure 14 indicates that the opposite is true. This is caused by the fact that the second mode being initially stable contains less bending energy and consequently builds up more slowly in comparison to the unstable first bending mode.

Figure 19 indicates that the nozzle deflections are high which in turn means large loads. These deflections and loads can be reduced by increasing the short period frequency. Gain-phase analysis verified that the increased short period frequency could be obtained with minor modifications to the control system compensation. With these modifications, the short period frequency could be increased from the .47 rad/sec shown in the trajectory run to .75 rad/sec. This increase in frequency would result in a significant reduction in the nozzle deflection and loads.

It is a general characteristic of the Spectral Identification Adaptive Control System that if a bending mode is well stabilized its excitation is low and the identification accuracy is poor. If, on the other hand the bending energy is high due to poor bending stability, the bending frequencies are well identified by the spectral system. It is this fact that guarantees stability with a properly designed basic control system because the mor unstable and thus the more excited the bending mode becomes, the more accurate the identification and therefore the better assurance of a resultant stable configuration.

10 X 10 TO THE CENTIMETER 46 1517
KEUFFEL & ESSER CO.

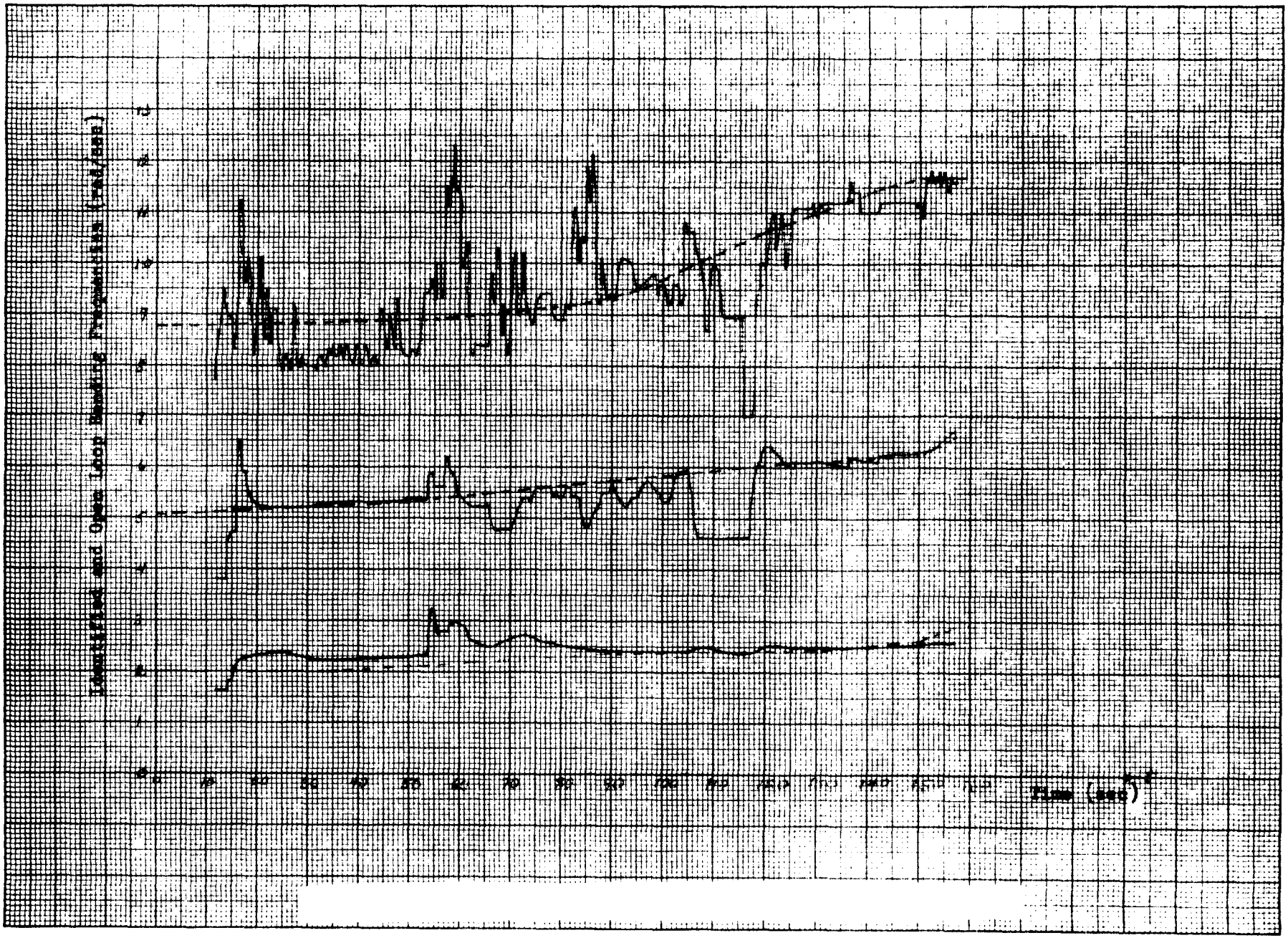

Figure 14. Identified And Open Loop Bending Frequencies Versus Time

K&E 10 X 10 TO THE CENTIMETER 46 1517
KEUFFEL & ESSER CO.

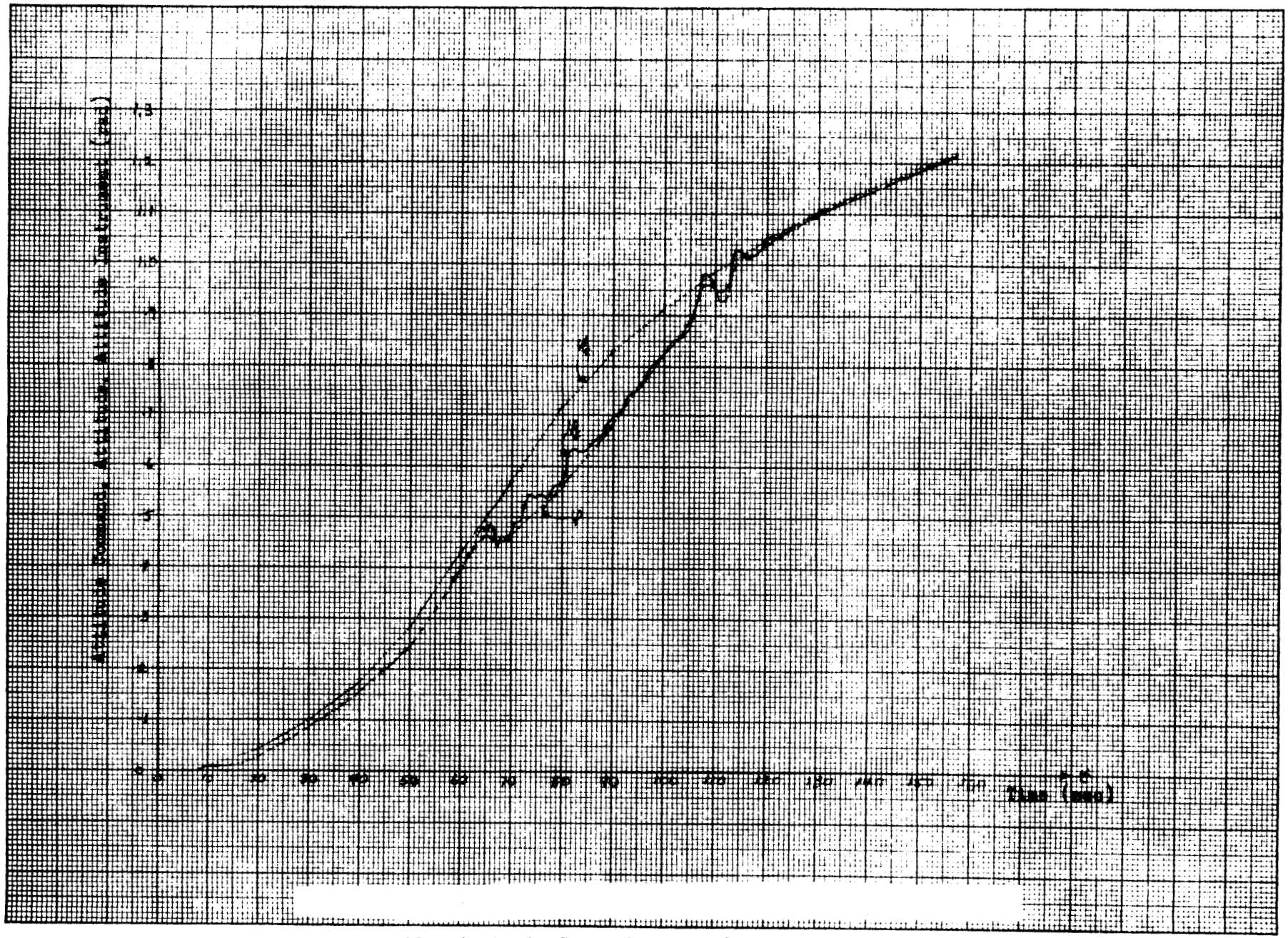

Figure 15. Attitude Command, Attitude Response and Instrument Output Versus Time

K&E 10 X 10 TO THE CENTIMETER 46 1517
KEUFFEL & ESSER CO.

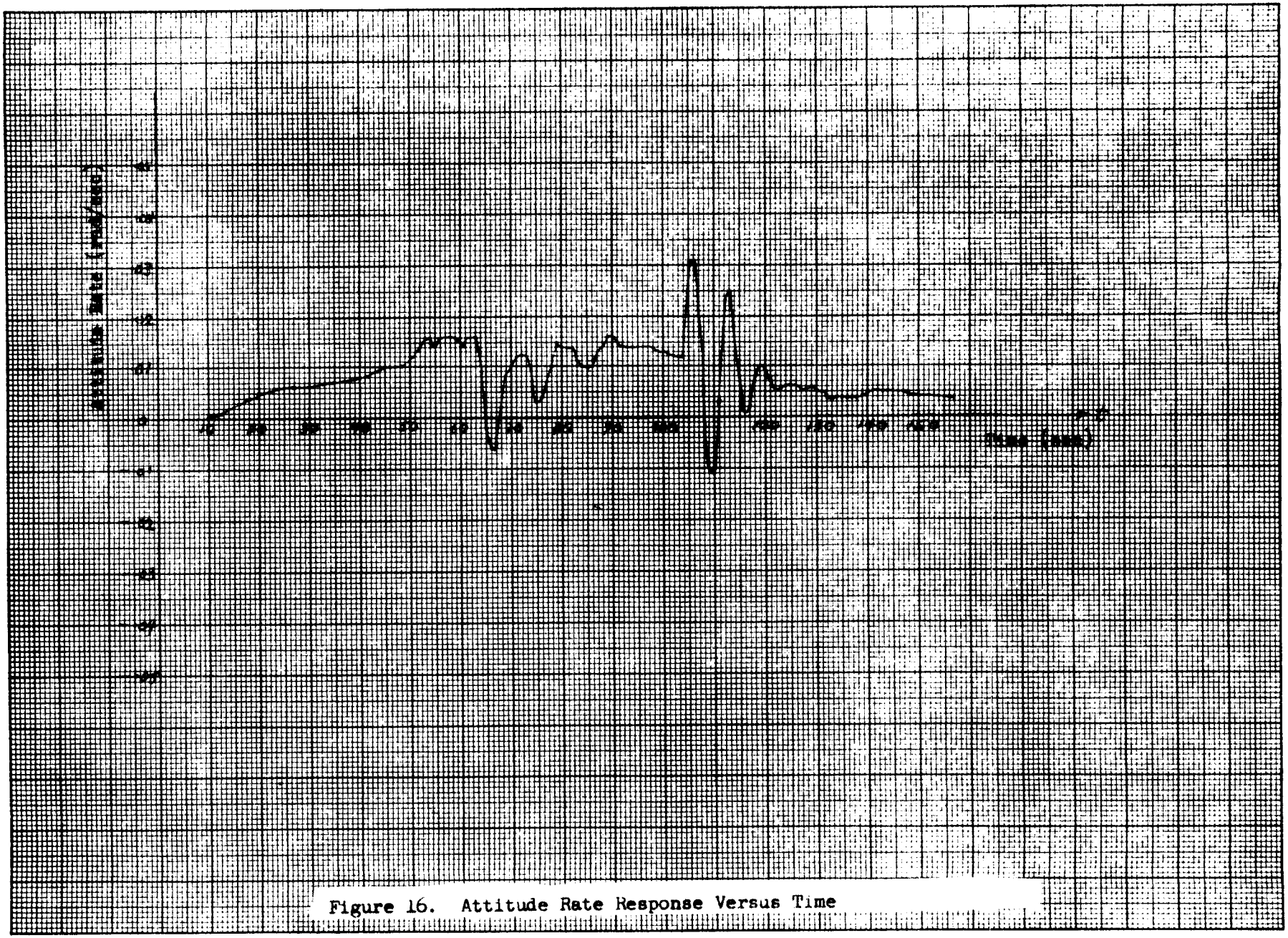

Figure 16. Attitude Rate Response Versus Time

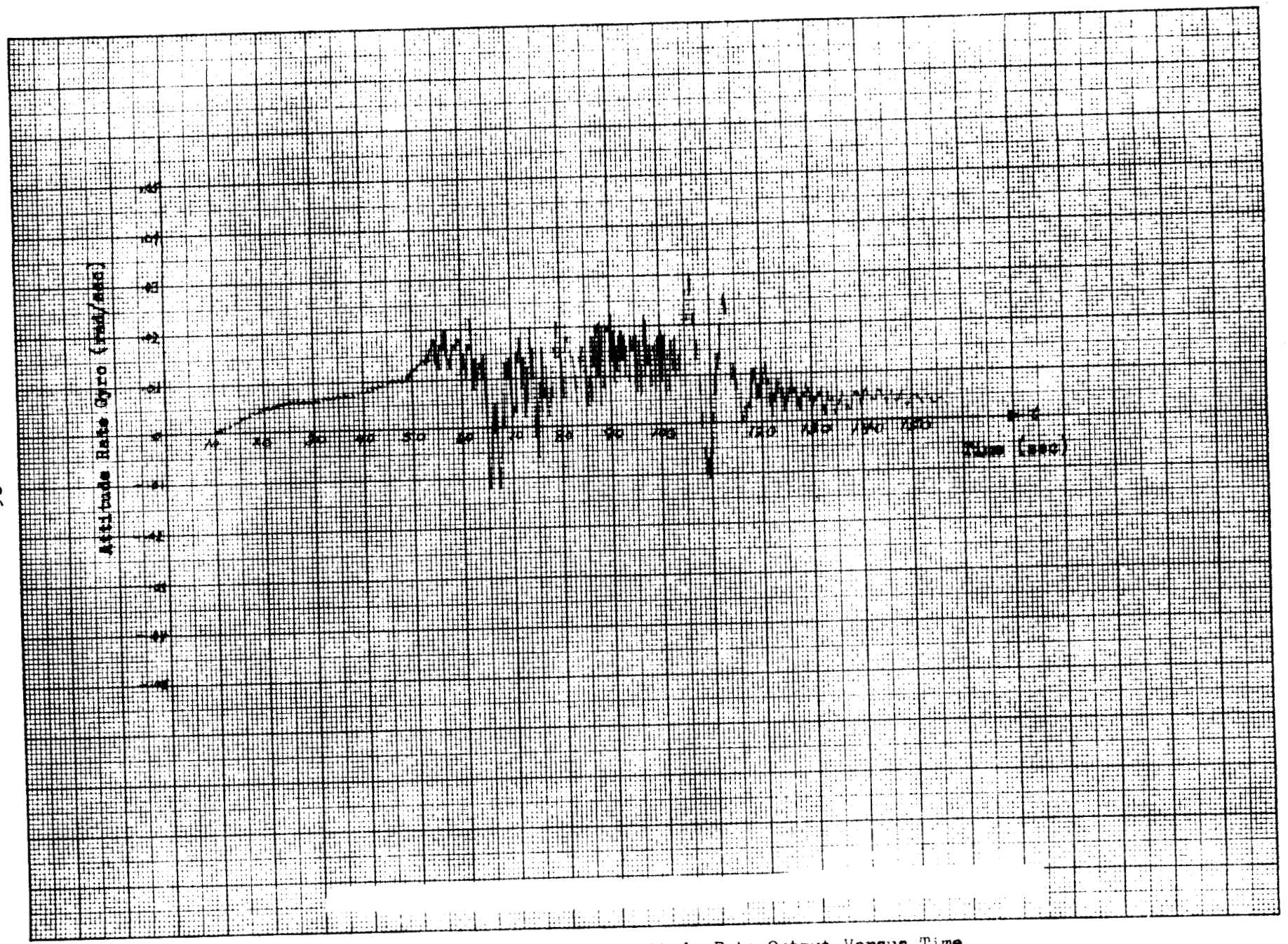

Figure 17. Instrument Attitude Rate Output Versus Time

K&E 10 X 10 TO THE CENTIMETER 46 1517
KEUFFEL & ESSER CO

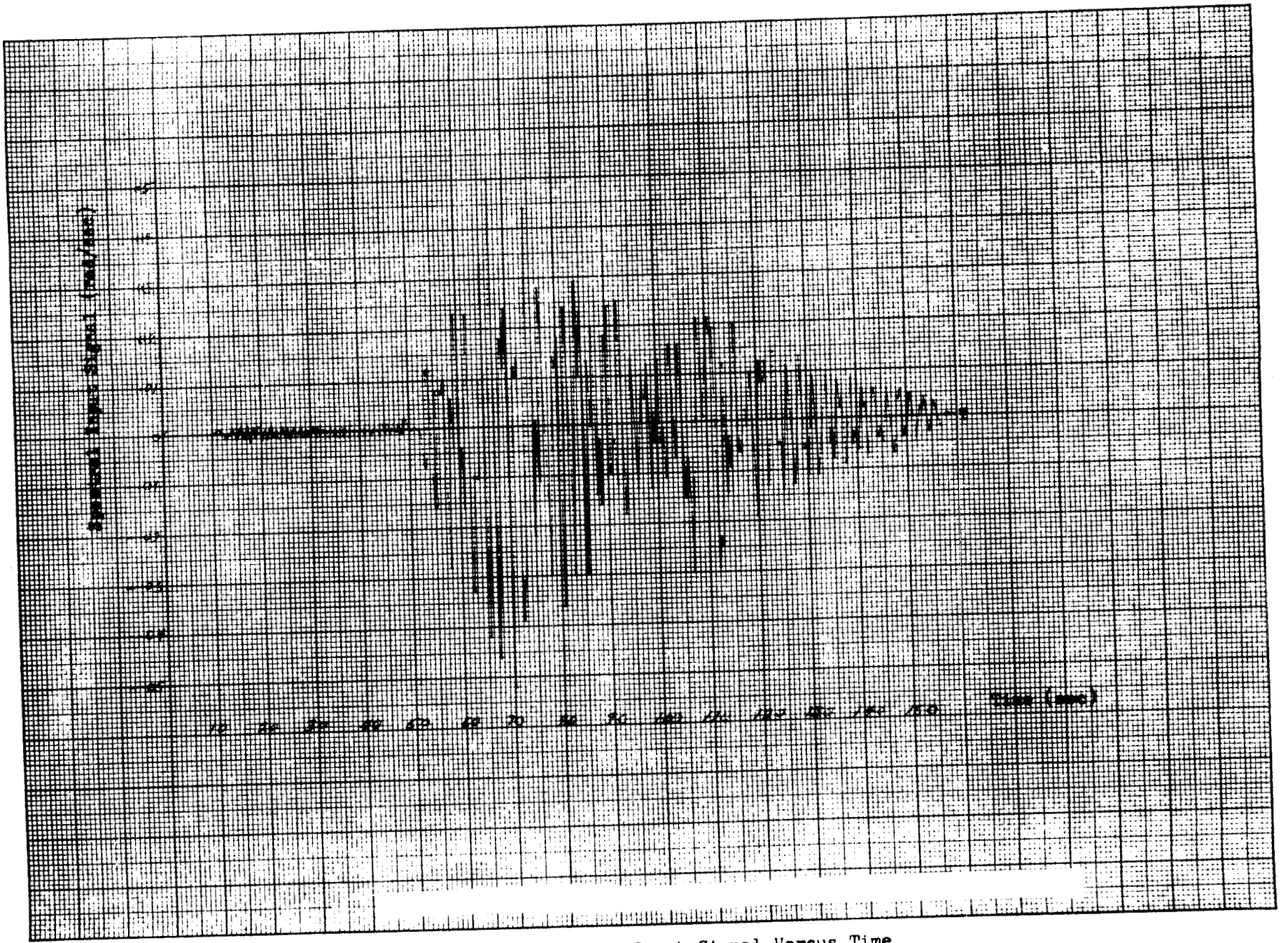

Figure 18. Spectral Filter Input Signal Versus Time

K&E 10 X 10 TO THE CENTIMETER 46 1517
KEUFFEL & ESSER CO.

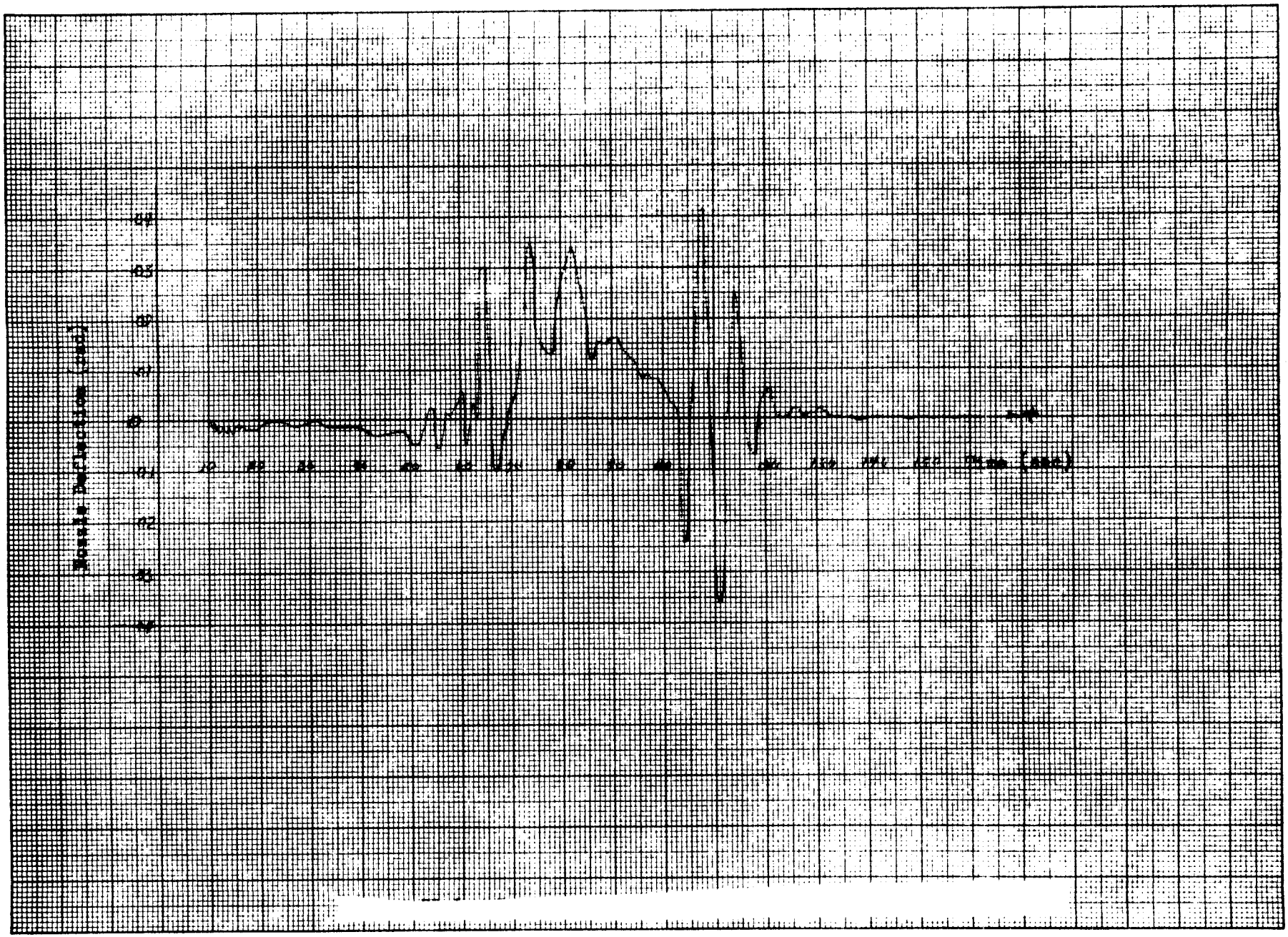

Figure 19. Nozzle Deflection Versus Time

K+E 10 X 10 TO THE CENTIMETER 46 1517
KEUFFEL & ESSER CO.

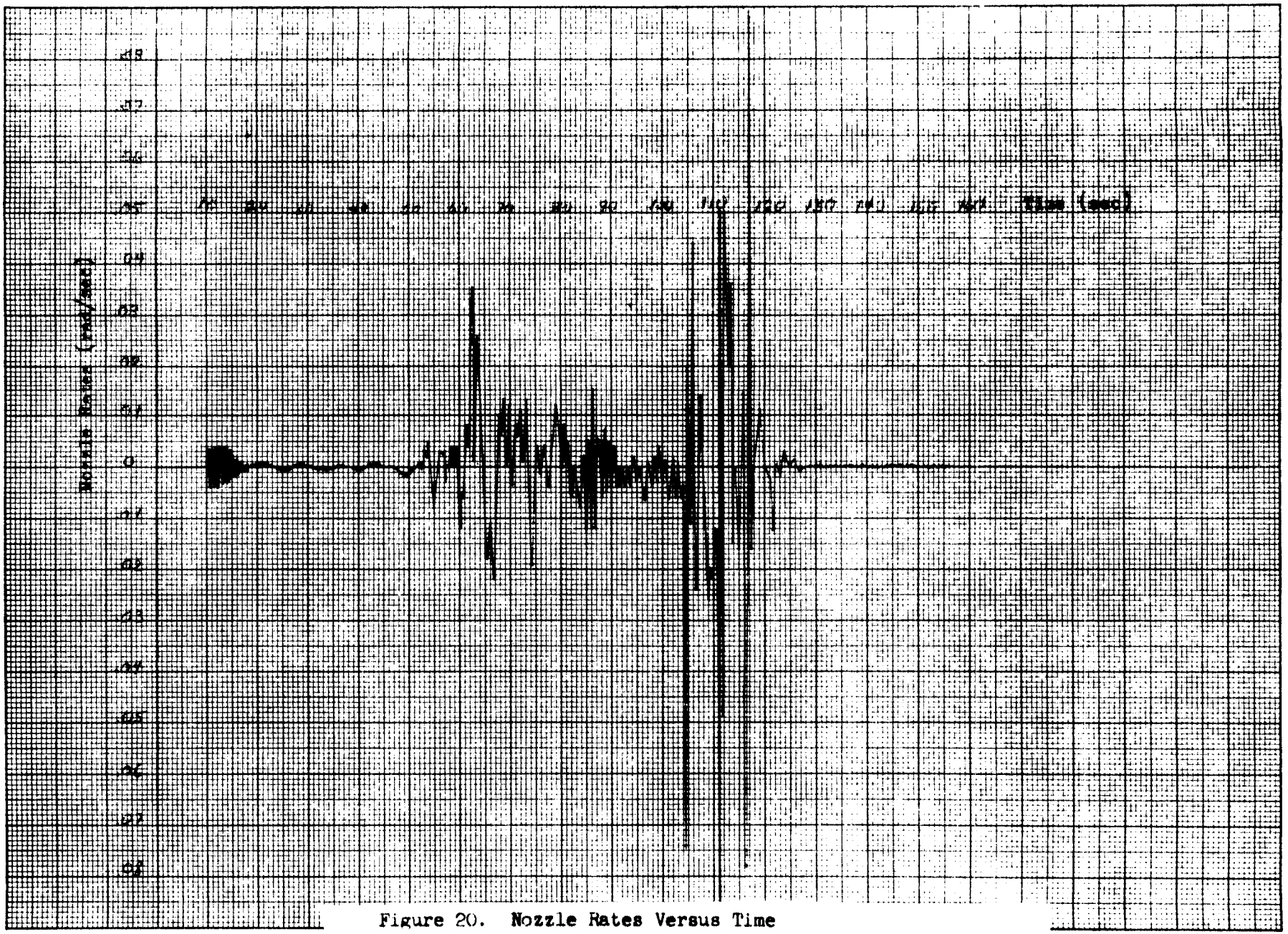

Figure 20. Nozzle Rates Versus Time

K&E 10 X 10 TO THE CENTIMETER 46 1517
KEUFFEL & ESSER CO

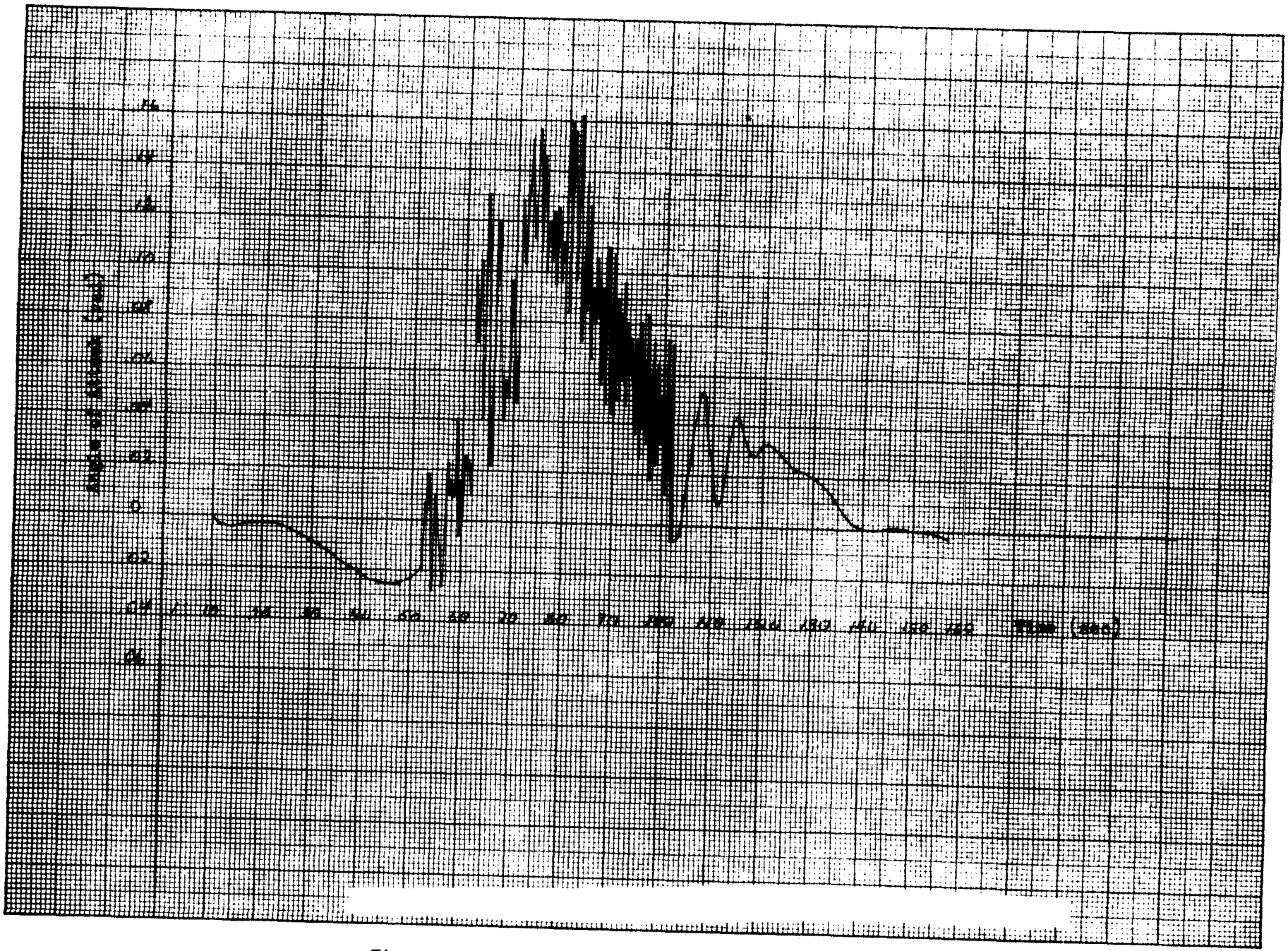

Figure 21. Angle of Attack Versus Time

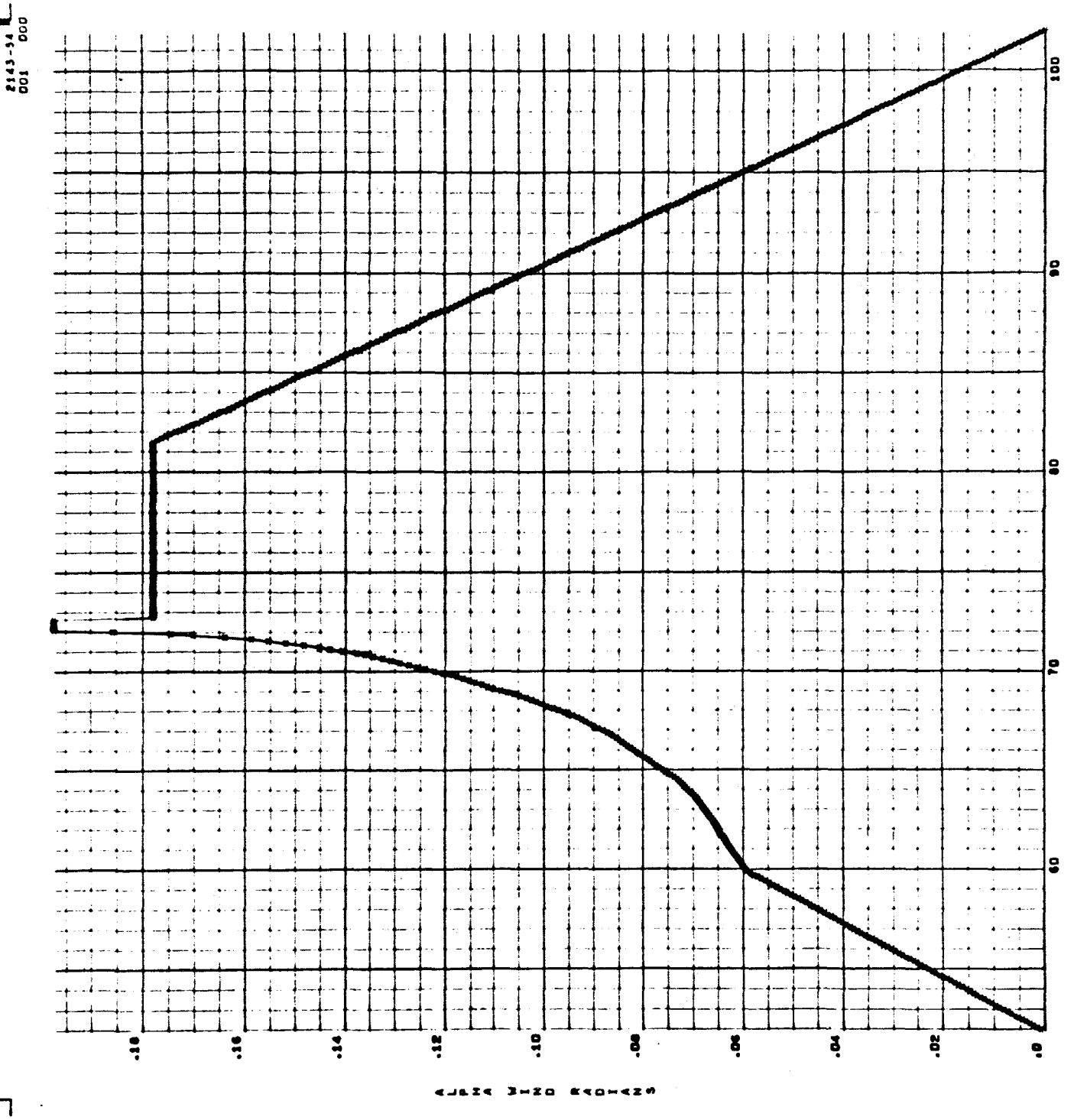

Figure 22. Worst Case MSFC Wind Profile

The third mode identification was, in general, poorer than either the first or the second mode identification in most of the simulation runs obtained. This can be attributed to several possible causes which are:

(1) There is an attenuation of high frequencies due to system lags and thus, the third mode energy is in general lower than the first and second mode energy.
(2) The spectral filter accuracy decreases as the number of samples per tuned frequency period decreases, thus the accuracy of the higher frequency spectral filters is not as high as the lower frequency spectral filters.
(3) The actual frequency being identified is the closed loop bending frequency which may shift more radically for the third bending mode.

A technique exists for eliminating at least partially the first two possible causes of poor third mode identification. This modification consists of combining the spectral integral filters with a differentiation on the spectral input signal. By taking the derivative of the spectral input signal a gain proportional to the square of the tuned frequency is obtained on each spectral filter thus eliminating partially the first cause for poor third mode identification. Equation 17 represents the integral over 1/2 period of the sqs ($\omega_o t$). The integration within the computer is accomplished by using rectangular integration which is the source of sampling errors. If the derivative of $E_{in}(t)$ is substituted into equation (17) for $E_{in}(t)$ then the exact value of the integral with no sampling error is given by equation (28).

$$S_i = -\int_{t_o}^{t_o + ip} (-1)^i \cdot \dot{E}_{in}(t)\, dt = E_{in}(t_o + p) - E_{in}(t_o) \qquad (28)$$

Thus, the integral can be evaluated exactly by taking samples of the input signal when the square wave changes sign.

Other trajectory runs were made where instrument noise and fuel slosh were included. Instrument noise caused increased bending activity because of increased nozzle activity due to the noise. The increased bending activity in turn caused better identification of the bending frequencies. The addition of fuel slosh also increased the bending activity but there appeared to be no tendency for the identifiers to identify the slosh frequency.

VII. CONCLUSIONS

The Spectral Identification Adaptive Control System has been demonstrated to be capable of controlling a realistic flexible vehicle with dynamic and flexibility parameter uncertainties. When operating in conjunction with a properly designed control system, stable performance is guaranteed. The more excited a bending mode becomes due to temporary instability the more accurately it is identified and thus, the greater assurance of obtaining a stabilizing control system. The system has been studied with up to 25% initial uncertainty and has performed well enough to assure that stable operation is achieved independent of initial uncertainty.

The system maintains its performance in the presence of a realistic environment of winds and instrument noise. It maintains stable control during the operation of a conventional load relief system.

The Spectral Identification Adaptive Control System must be designed around the vehicle it is to control. Obviously the frequencies at which the spectral filters are set must be over the total range of possible bending frequencies. The control system must be designed to give adequate short period response plus the assurance that at no time can the condition exist where a notch filter placed at an identified frequency will cause the vehicle to have an unstable mode at that frequency.

In summary, the spectral identification adaptive control system offers both a practical (mechanization) as well as a performance (stability and trajectory) solution to the control problem of large launch vehicles. The main features of the system is its versatility to handle a wide variety of payload and/or mission changes by digital software (programming) techniques as opposed to analog hardware modifications.

The system operates with only a minimum of a priori knowledge of the vehicle dynamics and the system can be readily adjusted to meet changes in control system requirements. The digital computer requirements of the system are within the capability of present day technology. Finally the spectral identification adaptive control, by virtue of the factors previously stated, affords a truly cost effective approach to the design of an integrated control system (guidance/control/loads/structure) for future large launch vehicles.

VIII. APPENDIX

This section includes the basic equations of motion and pertinent vehicle bending data used in the study.

EQUATIONS OF MOTION

Moment Equation

$$\ddot{\phi} = \frac{-C_{Z_\alpha} q A \left(X_{cg} - C_{cp}\right)\alpha}{I_{XX}} - \frac{F\left(X_{cg} - X_\beta\right)}{2 I_{XX}} \beta$$

$$+\frac{F\left(X_{cg} - X_E\right)}{I_{XX}} \sum_i Y_i' \left(X_\beta\right) \eta_i - \frac{F}{I_{XX}} \sum_i Y_i \left(X_\beta\right) n_i$$

$$+\sum_j \frac{\ell_{s_j} m_{s_j}}{I_{XX}} \ddot{Z}_{s_j} + \sum_j \frac{F - X}{m I_{XX}} m_{s_j} Z_{s_j} \qquad (1)$$

$$- \left[\frac{\left(X_{cg} - X_\beta\right) S_E}{I_{XX}} + \frac{I_E}{I_{XX}}\right] \ddot{\beta} - \frac{(F - X)\, S_{E_\beta}}{m I_{XX}}$$

Forces Normal to Velocity

$$\dot{\alpha} = \frac{-(F - X)\alpha}{m V_o} - \frac{F}{2 m V_o} \beta - \frac{C_{z_\alpha}}{m V_o} q A \alpha$$

$$+\frac{F}{m V_o} \sum_i Y_i' \left(X_\beta\right) \eta_i = \sum_j \frac{m_{s_j} \ddot{Z}_{s_j}}{m V_o} + \dot{\phi} - \frac{g \sin\left(\phi - \alpha\right)}{V_o} \qquad (2)$$

Bending Equation

$$\ddot{\eta}_i + 2\zeta_i W_i \eta_i + W_i^2 \eta_i = \frac{F Y_i \left(X_\beta\right)}{2 m_i} \beta + \frac{S_E Y_i \left(X_\beta\right) + I_E Y_i \left(X_\beta\right)}{m_i} \ddot{\beta}$$

$$- \sum \frac{m_{s_j}}{m_i} \left[Y_i\left(X_{s_j}\right) \ddot{Z}_{s_j} + \frac{F-X}{m} + Y_i'\left(X_{s_j}\right) Z_{s_j} \right]$$

$$+ \left[\int^{x} \frac{\partial C_{Z\alpha}}{\partial X} Y_i(X) dX \right] \frac{q\,A}{m_i} \alpha \tag{3}$$

Slosh Equation

$$\ddot{Z}_{s_j} + 2\zeta_{s_j} W_{s_j} \dot{Z}_{s_j} + W_{s_j}^2 Z_{s_j} = \ell_{s_j} \ddot{\phi} - \frac{F}{2m} \beta - \frac{C_{Z_\alpha} q\,A}{m} \alpha$$

$$+ \sum \frac{F}{m} Y_i'(X_\beta) \eta_i + \sum_j \frac{m_{s_j}}{m} \ddot{Z}_{s_j} \tag{4}$$

$$- \sum_i \left[Y_i\left(X_{s_j}\right) \ddot{\eta}_i + \frac{F-X}{m} Y_i\left(X_{s_j}\right) \eta_i \right]$$

Sensor Equations

$$\Phi_I = \Phi - \sum_i Y_i' \left(X_{\Phi_I}\right) \eta_i \tag{5}$$

$$\dot{\Phi}_I = \dot{\Phi} - \sum_i Y_i' \left(X_{\dot{\Phi}_I}\right) \dot{\eta}_i \tag{6}$$

$$N_Z = \frac{F}{2m} \beta + \frac{C_Z \alpha\, q\, A}{m} \alpha - \left(X_{cg} - X_{N_z}\right) \ddot{\Phi} + \sum_i Y_i \left(X_{N_z}\right) \ddot{\eta}_i \tag{7}$$

$$- \sum_i \frac{F}{m} Y_i'(X_\beta) \eta_i - \sum_i \frac{m_{s_j}}{m} \ddot{Z}_{s_j}$$

Control Equation

$$\beta_c = K_\phi \left(-\phi_c + \phi_I + K_{\dot{\phi}} \dot{\phi}_I + K_{N_z} N_Z \right)$$

Figures 23, 24, 25 and 26 show the bending slopes at the rate gyro location, bending slopes at attitude gyro location, differential slopes for instruments located at 120.54 and 46.54 meters and bending frequencies as a function of time respectively.

Symbols

I_{XX}	pitch moment of inertia
C_{Z_α}	normal force coefficient
X_{cg}	location of vehicle Cg
X_{cp}	location of vehicle CP
X_β	location of vehicle gimbal point
q	dynamic pressure
A	cross sectional reference area
F	total thrust
X_E	location of nozzle cg
$Y_i'(X_\beta)$	normalized bending slope at X_β
$Y_i(X_\beta)$	normalized bending displacement at X_β
ℓ_{s_j}	distance from vehicle cg to slosh mass cg
m_{s_j}	slosh mass
X	drag force
S_E	first moment of swivel about gimbal point

I_E	engine moment of inertia about gimbal point
m	vehicle mass
V_o	vehicle velocity
δ_i	bending damping
W_i	bending frequency
$Y_i\left(X_{s_j}\right)$	bending displacement at slosh mass cg
$Y_i'\left(X_{s_j}\right)$	bending slope at slosh mass cg
$\int^{x} \frac{\alpha C_{Z_X}}{\alpha X} Y_i(X)dX$	normalized generalized force function
m_i	bending model mass
δ_{s_j}	slosh damping
W_{s_j}	slosh frequency
$Y_i'\left(X_{\phi_I}\right)$	bending slope at gyro location
$Y_i'\left(X_{\dot{\phi}_I}\right)$	bending slope at rate gyro location
$Y_i'\left(X_{N_Z}\right)$	bending slope at normal accelerometer location
$Y_i\left(X_{N_Z}\right)$	bending displacement at normal accelerometer location
X_{N_Z}	location of N_Z instrument

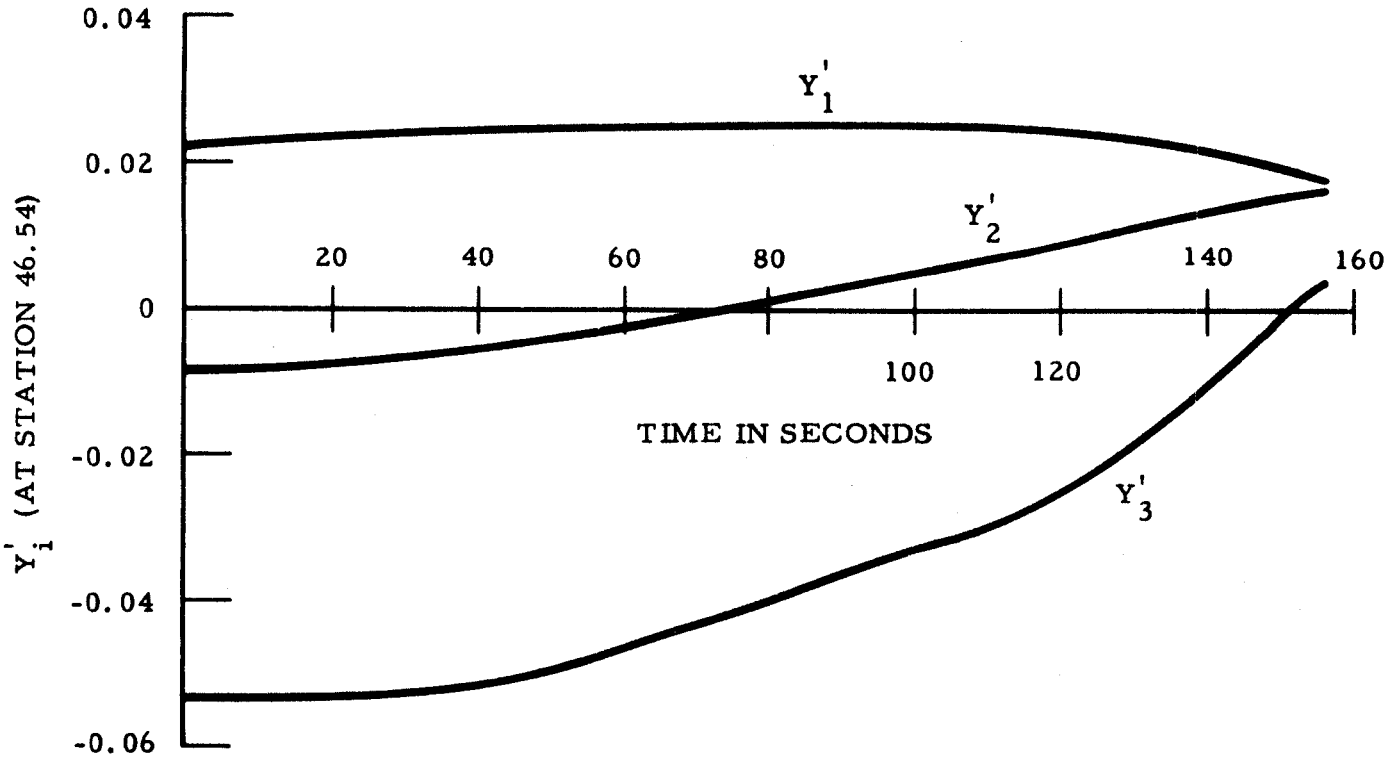

Figure 23. Bending Slopes at Rate Gyro Location

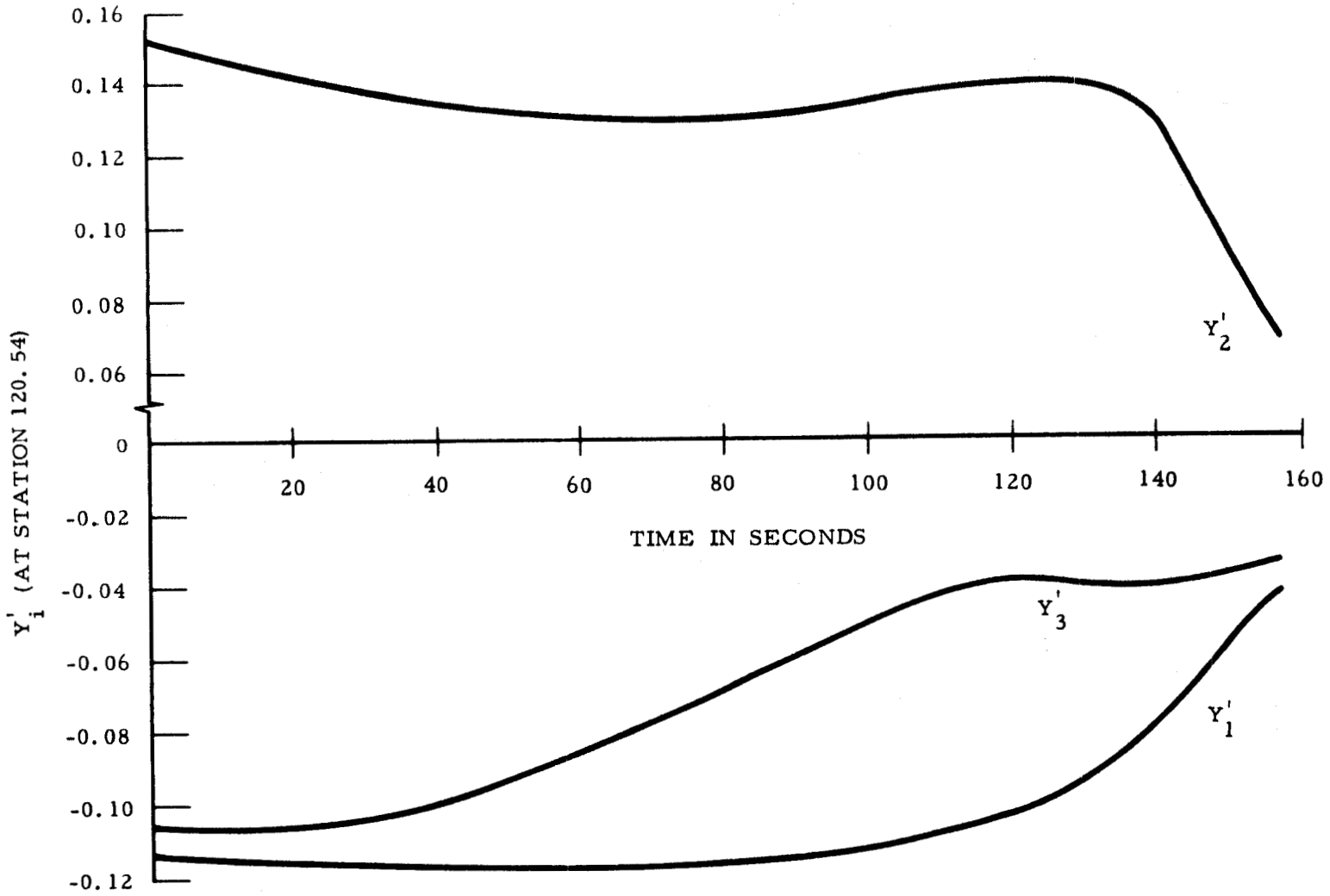

Figure 24. Bending Slopes Attitude Gyro Location

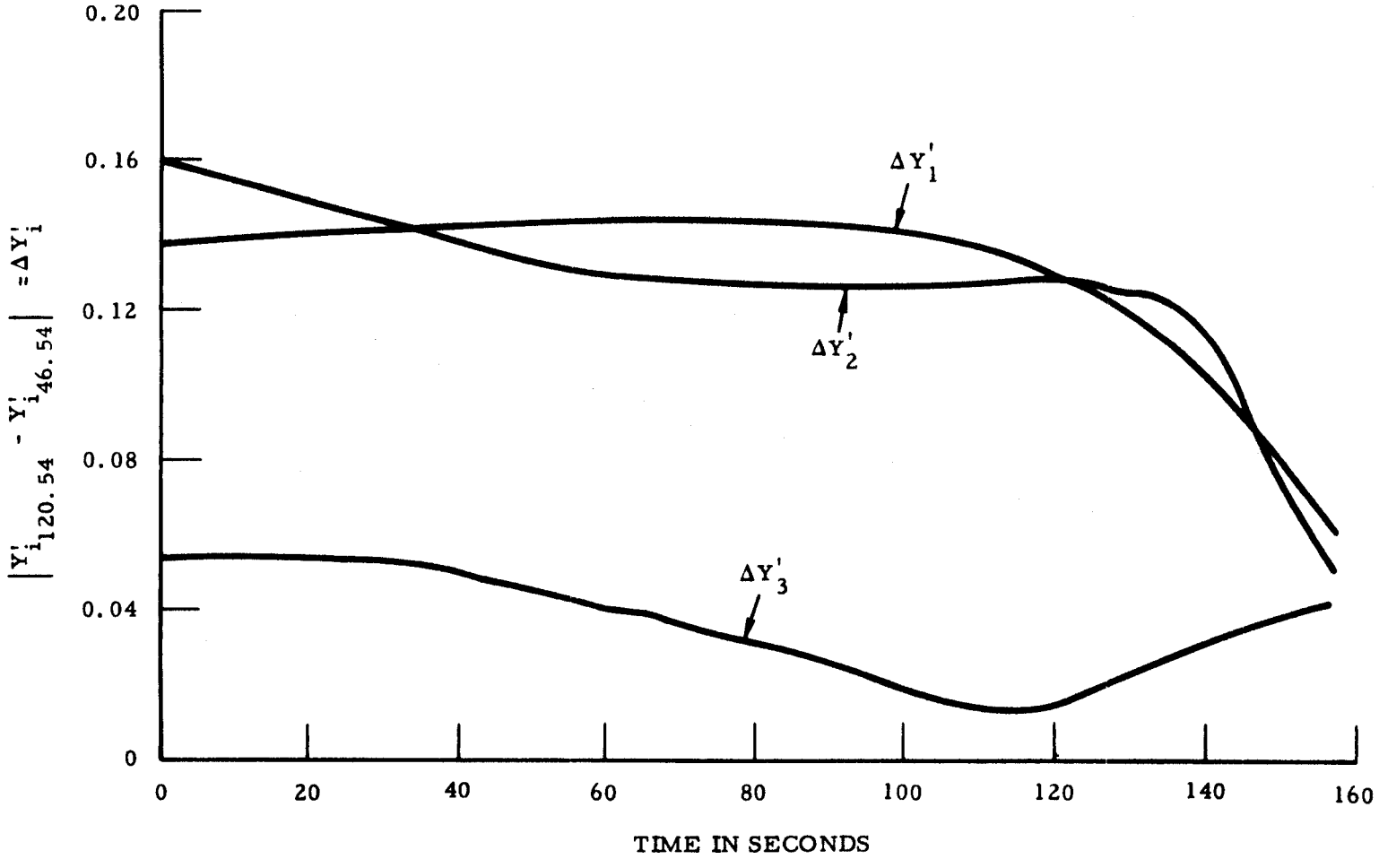

Figure 25. Magnitude of Differential Slopes for 120.54 and 46.54 Meters

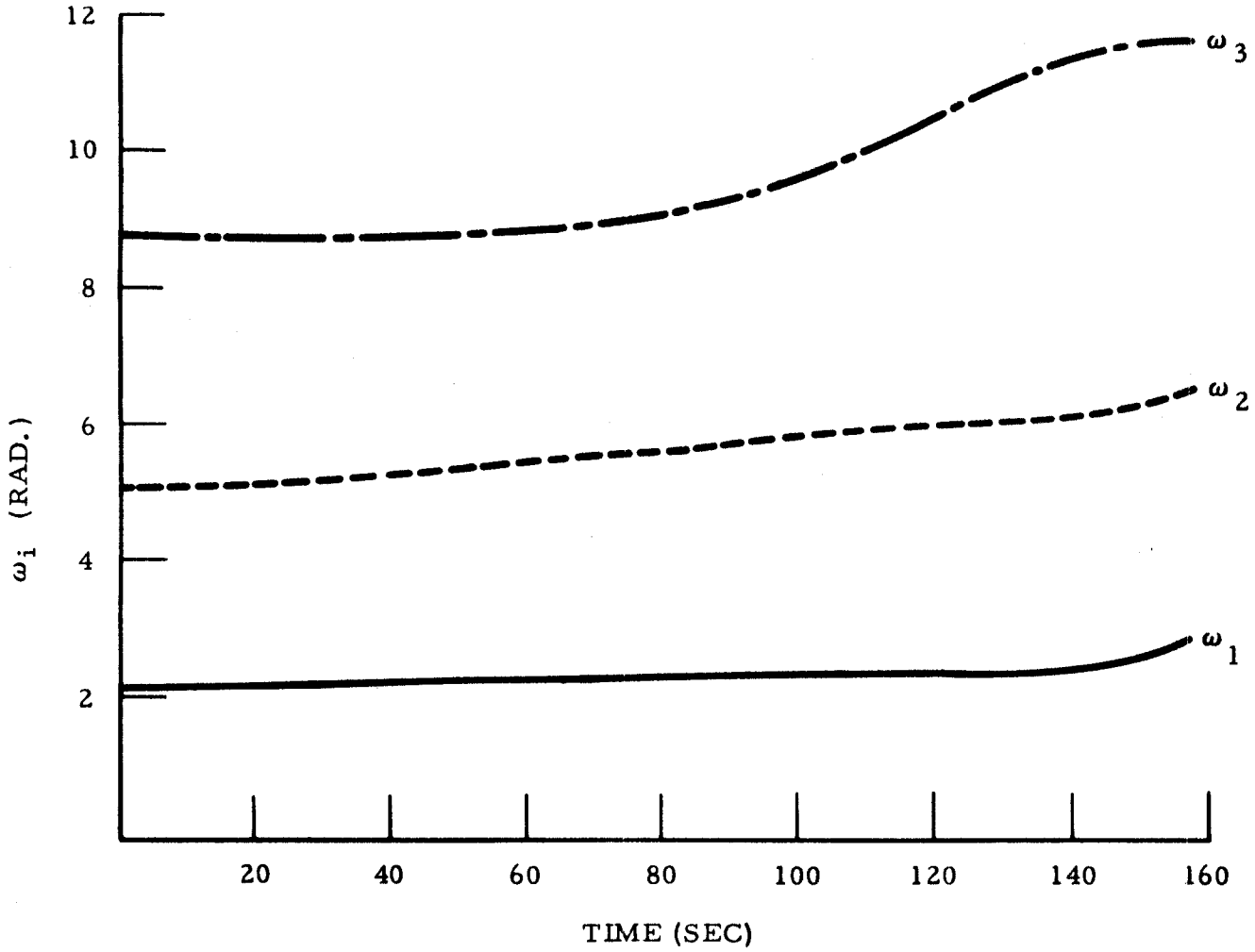

Figure 26. ω_i vs Time